Icarus 197 (2008) 291–306

Contents lists available at ScienceDirect

Icarus

www.elsevier.com/locate/icarus

Nonuniform cratering of the terrestrial planets

Mathieu Le Feuvre *, Mark A. Wieczorek

Institut de Physique du Globe de Paris, 4, avenue de Neptune, 94107 Saint-Maur, France

ARTICLE INFO

Article history:
Received 26 July 2007
Revised 28 March 2008
Available online 9 May 2008

Keywords:
Cratering
Terrestrial planets

ABSTRACT

We estimate the impact flux and cratering rate as a function of latitude on the terrestrial planets using a model distribution of planet crossing asteroids and comets [Bottke, W.F., Morbidelli, A., Jedicke, R., Petit, J.-M., Levison, H.F., Michel, P., Metcalfe, T.S., 2002. Icarus 156, 399–433]. After determining the planetary impact probabilities as a function of the relative encounter velocity and encounter inclination, the impact positions are calculated analytically, assuming the projectiles follow hyperbolic paths during the encounter phase. As the source of projectiles is not isotropic, latitudinal variations of the impact flux are predicted: the calculated ratio between the pole and equator is 1.05 for Mercury, 1.00 for Venus, 0.96 for the Earth, 0.90 for the Moon, and 1.14 for Mars over its long-term obliquity variation history. By taking into account the latitudinal dependence of the impact velocity and impact angle, and by using a crater scaling law that depends on the vertical component of the impact velocity, the latitudinal variations of the cratering rate (the number of craters with a given size formed per unit time and unit area) is in general enhanced. With respect to the equator, the polar cratering rate is about 30% larger on Mars and 10% on Mercury, whereas it is 10% less on the Earth and 20% less on the Moon. The cratering rate is found to be uniform on Venus. The relative global impact fluxes on Mercury, Venus, the Earth and Mars are calculated with respect to the Moon, and we find values of 1.9, 1.8, 1.6, and 2.8, respectively. Our results show that the relative shape of the crater size-frequency distribution does not noticeably depend upon latitude for any of the terrestrial bodies in this study. Nevertheless, by neglecting the expected latitudinal variations of the cratering rate, systematic errors of 20–30% in the age of planetary surfaces could exist between equatorial and polar regions when using the crater chronology method.

1. Introduction

Impact cratering is not only a major geologic process that shapes planetary surfaces (see Melosh, 1989), but it is also a method by which surfaces can be dated. In essence, a fresh surface will accumulate craters at a given rate, and the number of craters per square kilometer can be converted to an approximate age (e.g., Neukum et al., 2001; Stöffler and Ryder, 2001; Hartmann and Neukum, 2001). While certain regions of the Moon have been dated directly by the analysis of radiogenic isotopes in samples with known geologic context, for other planets, such as Mercury, Venus, and Mars, "crater counting" is one of the only reliable means for placing relative geologic stratigraphy into an approximate absolute framework.

When dealing with planetary cratering rates, and in particular when using this crater chronology method, it is commonly assumed that a given bolide is equally likely to impact at any location on the planet's surface. Furthermore, most studies also assume that the impact velocity and impact angle distributions are independent of position (e.g., Pierazzo and Melosh, 2000; Neukum et al., 2001; Strom et al., 2005). Given that the impact flux is assumed to be everywhere the same, and that the impact velocity and angle are also assumed not to depend upon position, the resulting cratering rate would also be independent of position.

The above assumptions would be expected to be true if the velocity distribution of candidate impactors were isotropic (e.g., Pierazzo and Melosh, 2000), or if the planet were sufficiently massive so that the trajectories of objects with high encounter velocities could be gravitationally deflected. However, the assumption of isotropy is questionable. Furthermore, many impactors have high enough approach velocities such that their trajectories are not significantly deviated by the planet. Indeed, in the case of zero inclination with respect to the equator of the planet, simple geometric considerations predict that objects with infinite approach velocities will produce an impact flux that varies with the cosine of the geocentric latitude. Conversely, if the average relative inclination of projectiles striking an object were extremely high, one would expect more impacts to occur (per unit area) at the poles.

With few exceptions (e.g., Morota and Furumoto, 2003; Morota et al., 2005; Zahnle et al., 2001) spatial variations of the cratering rate have not been considered when applying the crater chronology method. Assuming that the average cratering rate of a planet

* Corresponding author. Fax: +33 (0) 1 45 11 42 57.
E-mail address: lefeuvre@ipgp.jussieu.fr (M. Le Feuvre).

0019-1035/$ – see front matter
doi:10.1016/j.icarus.2008.04.011

Table 1
Selected nomenclature

a, e, i	Semi-major axis, eccentricity and inclination of a celestial object
i_{mut}	Mutual inclination: angle between the orbit planes of a planet and a planet-crossing object
$\mathbf{u}_\infty$	Relative orbital encounter velocity
i_∞	Inclination of $\mathbf{u}_\infty$ with respect to the planet's orbit plane
u	Impact velocity
θ	Impact angle with respect to the surface
λ	Latitude of impact
d, D	Planet-crossing object and crater diameters, respectively
$\Phi_b(>d)$	Average present day impact flux for bolides larger than a given size
$\varphi_b(\lambda)$	Latitudinal variations of the impact rate, normalized to the average value
$\varphi_c(>D,\lambda)$	Latitudinal variations of the cratering rate, for craters larger than a given size, normalized to the average value
$\dot{N}(>D,\lambda)$, $\dot{n}(D,\lambda)$	Cumulate and differential number of impactors, respectively, per unit time and area, as a function of latitude
$R_b(>d)$, $R_c(>D)$	Average impact and cratering rate with respect to the Moon
$r_b(\lambda)$	Latitudinal variations of the impact rate with respect to the Moon, normalized to the average value
$r_c(>D,\lambda)$	Latitudinal variations of the cratering rate with respect to the Moon, normalized to the average value

is constant with time, a latitudinal variation of the cratering rate of a certain percentage would translate directly into an age bias of the same magnitude. Given the importance of the crater chronology methodology in deciphering a planet's geologic evolution, it is important to quantify the magnitude of such an effect.

Halliday (1964) predicted latitudinal variations in the rate of meteorites falling on the Earth. However, this study was limited to the case of projectiles confined to the ecliptic plane with a limited number of encounter velocities. From the limited observations of fireballs provided by the Canadian camera network (MORP), Halliday and Griffin (1982) generated a set of synthetic orbits believed to be representative, and deduced among other results a pole/equator impact flux ratio of 0.85 on the Earth. Here we improve upon and extend this analysis to the terrestrial planets, using a realistic population of impactors (Bottke et al., 2002). In Section 2.1, we describe how we calculate for each planet the encounter conditions from the planet-crossing population model. Next, in Section 2.2, using this encounter probability distribution, we analytically calculate the impact rate on the planet's surface under the approximation that the gravitational attraction of the Sun can be neglected during the encounter phase. In Section 3 we discuss our results in terms of impact flux and cratering rates, given scaling laws that relate crater size to the impact velocity and impact angle. In Section 4 we quantify the sensitivity of these results, and discuss how they compare with some observations. A selected nomenclature of the more important variables used in this study is given in Table 1.

2. Method

In order to estimate the latitudinal variations of impact rates, impact velocities, and impact angles, we divide the problem in two steps. First, given an appropriate model of impactors in terms of semi-major axis a, eccentricity e and inclination i, we determine the impact probability distribution as a function of the relative encounter velocity and of the encounter inclination with respect to the orbital plane of the planet. Second, using these probabilities, we analytically calculate the trajectories of the impactors, account for the planet's obliquity, and determine the coordinates, velocity and incidence angle of each impact. This second step is performed in the framework of the 2-body problem, and ignores the gravitational influence of the Sun.

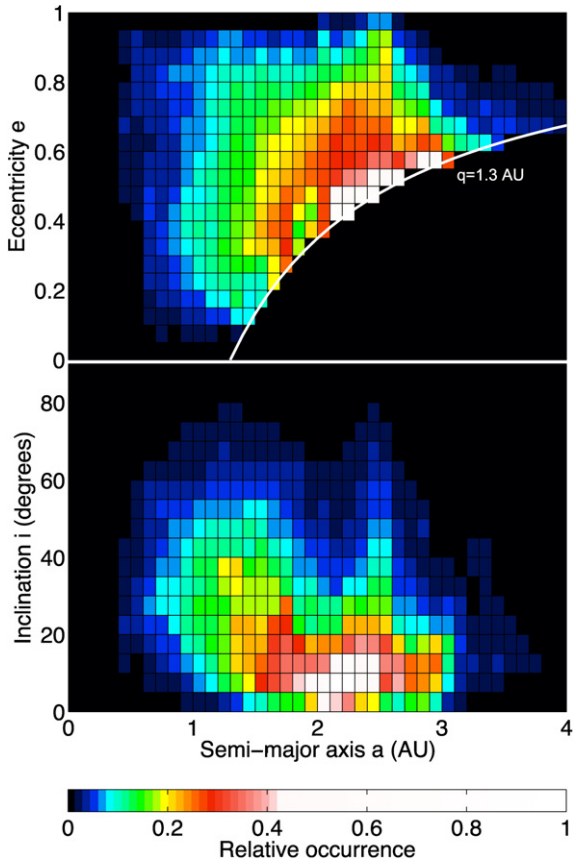

Fig. 1. NEO orbital element distribution from Bottke et al. (2002). (Top) Relative number of objects as a function of the eccentricity and semi-major axis. (Bottom) Relative number as a function of the inclination and semi-major axis. Objects with perihelia larger than 1.3 AU (white curve) are not plotted, so this population is not a complete representation of the objects that cross Mars.

2.1. Planetary encounter probabilities and conditions

We start with the debiased population of near Earth objects (NEOs) from Bottke et al. (2002). This distribution has been determined by numerical simulations of test particles coming from five intermediate source regions: the ν_6 resonance (boundary of the inner main belt fed by the adjacent material), the intermediate Mars-crossers bordering the main belt, the 3:1 mean motion resonance with Jupiter, the outer main belt, and the transneptunian disk (including both active and inactive Jupiter-family comets). This model has been calibrated by fitting a linear combination of these source regions to the real population observed by Spacewatch, after taking into account the observational bias. The Bottke et al. model assumes that the population of small bodies is currently in steady state.

Fig. 1 shows the number of objects in the orbital element space, $N(a,e,i)$, from the Bottke et al. model that reproduce the observed NEO population. We note that this model is discretized in 5° of inclination, 0.1 AU in semi-major axis, and 0.05 in eccentricity. One should be aware that the Bottke et al. model does not consider the isotropic comets, as no such discoveries with perihelia less than 1.3 AU were made by the Spacewatch survey. The affects of isotropic comets on our results will be discussed in Section 4.1.

As the vast majority of objects that encounter the terrestrial planets are derived from the asteroid belt and outer Solar System, and as there is no known source of objects within the orbit of Mars, the population of objects plotted in Fig. 1 should be also applicable to Mercury and Venus. While Bottke et al. did not explicitly account for Mercury when constructing their NEO model,

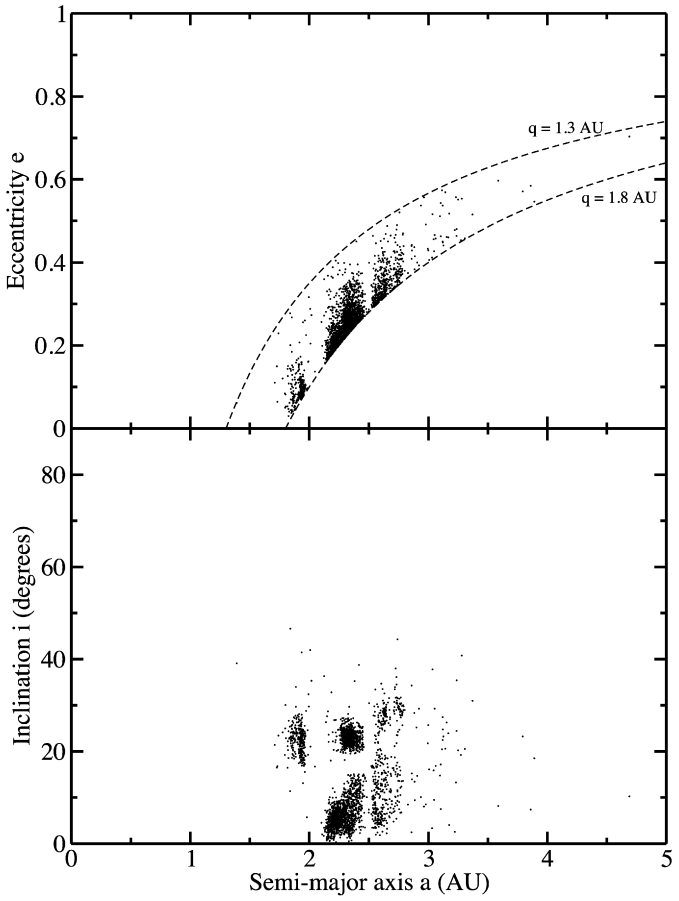

Fig. 2. Observed objects with $1.3 < q < 1.8$ AU and $H < 15$. For clarity, three objects with semi-major axes greater than 5 AU are not shown.

Marchi et al. (2005) argue that this neglect should not significantly affect the orbital dynamics of planet crossing objects nor the impact rates.

The NEO model can not be directly applied to Mars as it does not include all of the Mars-crossing objects. In order to account for these, it will be assumed that the observation of objects with perihelia q larger than 1.3 AU and magnitudes H smaller than 15 is relatively complete and representative of the orbital distribution of smaller objects (see Ivanov, 2001). These objects are tabulated in the file *astorb.dat*[1] compiled by E. Bowell and shown in Fig. 2 as of January 2007. The upper bound for Mars-crossing objects is taken at about $q < 1.8$ AU, which corresponds to the maximum martian eccentricity of about 0.2 that could occur over the past 3 Ga (Laskar et al., 2004a). A model for the planet-crossing objects (PCOs) that is applicable to Mars was constructed by combining the observed Mars-crossers for $q > 1.3$ AU with the Bottke et al. NEO model for $q < 1.3$ AU. As shown in Fig. 3, the Bottke et al. model was uniformly scaled such that the two models were coincident at $q = 1.3$ AU.

It is assumed that no correlations exist between the magnitude of an object and its orbital elements, as stated by (Stuart, 2001) for $H < 22.5$. This implies that the objects are large enough not to be significantly affected by the Yarkovsky effect (a size-dependent solar radiation pressure effect) during their collision lifetime (see Michel and Yoshikawa, 2005). We consider that this assumption is valid for the entire cratering population considered here, that is, objects that will produce craters larger than a kilometer. We also

[1] www.lowell.edu.

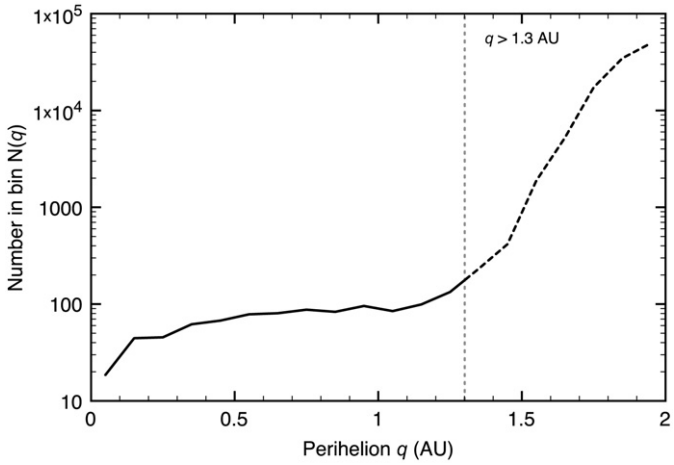

Fig. 3. Number of planet-crossing objects as a function of perihelion (bins of 0.1 AU). The NEO model (solid line) has been combined with the observed objects with $q > 1.3$ AU and $H < 15$ (dashed line), and scaled such that the two distributions are continuous at $q = 1.3$. The combined model is scaled to the estimated total number of objects with $H < 18{,}960$, from Bottke et al. (2002).

assume that the albedos of the planet crossing objects do not vary as a function of the orbital elements, and this allows us to convert an object's relative magnitude to a diameter using a single average albedo. While this is not completely correct (see Morbidelli et al., 2002; Stuart and Binzel, 2004) we will ignore this complication here.

The first step of our analysis is to calculate the probability that an object with the orbital elements (a, e, i) will impact a given planet, and to determine under what encounter geometries these impacts will occur. Since all of the planets in this study are rotating, the impact flux and cratering rate will only depend on latitude. This simplifies the analysis of the encounter geometry, as it will only be necessary to consider the angle between the relative encounter velocity vector and the orbit plane, as well as the magnitude of the relative encounter velocity.

We use the method of Greenberg (1982) and Bottke and Greenberg (1993), which is based on the approach of Öpik (1951) and Wetherill (1967), where it is assumed that the apsides and nodes of all bodies precess uniformly. This method explicitly accounts for the eccentricity of the target planet. The impact probabilities relate to the fraction of time during which the two bodies are close enough for a collision to occur (this corresponds to encounters with an impact parameter less than the radius of the planet's gravitational cross section). As is described more fully in Appendix A, individual (a, e, i) triads from our combined model of Fig. 1 and Fig. 2 are chosen randomly, then the probabilities of impact and corresponding encounter conditions are computed for a random orientation of the two orbits. These probabilities are then weighted by the proportion of objects in the corresponding cell of the PCO model. By repeating this procedure, we obtain a probability distribution as a function of the relative encounter velocity, u_∞, and of the inclination of $\mathbf{u}_\infty$ with respect to the orbit plane, i_∞. For convenience, we will simply refer to i_∞ as the "encounter inclination" in the following. We insist on the fact that the encounter conditions account for the orbital velocity of both the planet and planet-crossing object.

The impact probability between an object and a planet is proportional to $1/\sin i_{\mathrm{mut}}$, where i_{mut} is the inclination between the two orbit planes (see Appendix A). The mutual inclination varies between $i_0 - i$ and $i_0 + i$ (where i_0 and i are the inclinations of the planet and bolide, respectively) as a result of the precessing orbit planes of the two objects. When both inclinations are significant, the time spent when i_{mut} is zero is small. However, for the

Earth, whose orbital inclination is currently zero, the probability of an impact occurring rapidly increases as i approaches zero, and one would expect a corresponding depletion of objects in the NEO model. This depletion is not taken into account in the discretized version of the Bottke et al. model as shown in Fig. 1.

We model this expected depletion of planet crossing objects only for Earth-crossers with inclinations less than 5° (i.e., the smallest inclination bin in the Bottke et al. model). To do this, we assume that the change in number of objects at any given set of (a, i, e) is described by the equation

$$\frac{dN}{dt} = -PN + F, \tag{1}$$

where P is the probability of an impact occurring, and F is the rate of replenishment of objects into this phase space. By assuming steady state, it is easily shown that the number of objects will asymptotically approach F/P. If we next assume that F is a constant for a small range of values in (a, e, i) space, then the number of objects as a function of inclination should be proportional to $1/P$, or explicitly,

$$N(a, e) = C \sin i, \tag{2}$$

where C is determined by setting the total number of objects with $i < 5°$ equal to the value from the Bottke et al. model. This approximation is found to be in rough agreement with a computation of the residence times between 0 and 5° for about 10,000 test particles coming out of the inner main belt (W. Bottke, private communication). This is also in excellent agreement with the observations taken from the file *astorb.dat*. For inclinations greater than 5°, or for objects that are not crossing the Earth's orbit, the number of objects within an (a, e, i) cell should not vary much, and we use the average values per bin as plotted in Fig. 1.

2.2. Analytic determination of the impact conditions

In this section, we semi-analytically calculate the impact flux (number of impacts per unit time and unit area) on a planet's surface in the context of the two body problem. Since all of the terrestrial planets are rotating, if we neglect the possible complications of plate tectonics and true polar wander, the average impact flux should only depend upon latitude. We can therefore assume that all incoming trajectories come from the same direction in space, and subsequently average the number of impacts over longitude. For a synchronously-locked satellite, such as the Moon and the satellites of Jupiter, a superposed longitudinal effect may also be present (e.g., Morota and Furumoto, 2003; Shoemaker and Wolfe, 1982; Horedt and Neukum, 1984; Zahnle et al., 2001). This effect will not be addressed in this paper, and more detailed calculations for the Earth–Moon system will be presented in a forthcoming paper.

In the previous section, we have described how to determine the relative encounter velocity and encounter inclination probability distributions of the objects that impact the terrestrial planets. These encounter velocities and inclinations (with respect to the planet's orbital plane) have been calculated by assuming that the orbits of the planet and the planet-crosser were only influenced by the Sun. Here, it is assumed that during the encounter phase, the trajectory of the impactor is not influenced by that of the Sun, and that the projectile as seen by the planet approaches from an infinite distance. It is then straightforward to obtain analytic relations describing the latitudes of impact, impact velocities and incidence angles for each encounter inclination and encounter velocity (see Appendix B). As a test of the appropriateness of an initial approach distance set to infinity, we have run simulations using initial approach distances set to the planet's Hill sphere, and half of this value. The results of these tests were found to be nearly identical.

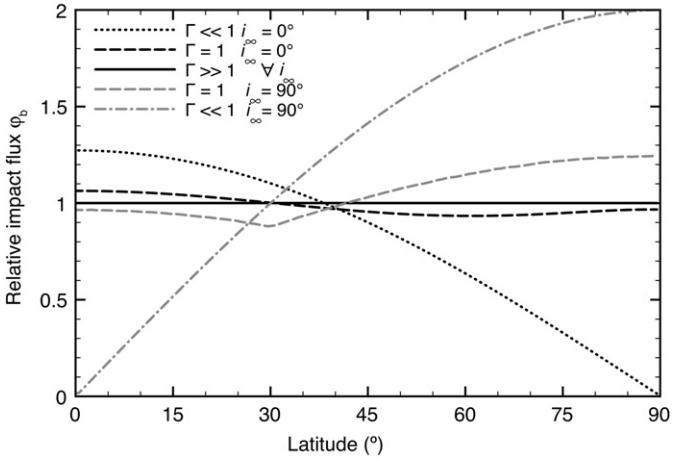

Fig. 4. Predicted impact flux as a function of latitude (normalized to the global average) when the encounter inclination is exactly 0 or 90°, and for a variety of values for Γ.

The impact flux, impact velocity distribution, and incidence angle distribution are calculated as a function of latitude in the following manner. First, an encounter inclination and velocity are taken from the (u_∞, i_∞) probability distribution as described in the previous section. The corresponding object will impact the planet as long as its impact parameter b is less than the gravitational cross section radius τ (see Fig. B.1), and we launch it within the corresponding area at a random location. To obtain a uniform spatial distribution, it is sufficient to take $b^2 = x\tau^2$, where x is a random number between 0 and 1, and to assume a random angular position within the disk. Next, using the relative encounter velocity, encounter inclination, launch position, and a random orientation of the planet's precessing spin axis, we determine the impact position and geometry. Finally, by repeating the above steps, and averaging over longitude, we obtain the latitudinal dependency of the impact flux, impact velocity and incidence angle.

Before presenting our results for the terrestrial planets, it will be instructive to demonstrate how latitudinal variations depend upon the encounter velocity and the planet's mass and radius. For illustrative purpose, we will here consider two end-member cases. First, we consider that the relative approach velocity of the projectiles is parallel to the equatorial plane, that is, both the encounter inclination and planet's obliquity are zero ($i_\infty = 0°$ and $\epsilon_0 = 0°$). Second, we consider that the approach velocity is perpendicular to the equatorial plane ($i_\infty = 90°$ and $\epsilon_0 = 0°$). For these specific cases, where i_∞ is fixed, the impact flux can be shown to depend only upon a single dimensionless parameter (see Appendix B):

$$\Gamma = \frac{GM_0}{R_0 u_\infty^2}, \tag{3}$$

where R_0 and M_0 are the radius and mass of the planet, and G is the gravitational constant. This parameter is simply proportional to the ratio of gravitational potential energy at the surface of the planet to the object's initial kinetic energy.

When the encounter velocity is very large with respect to the mass of the planet, Γ is close to zero, and the trajectories of the impactors are barely influenced by the gravitational field of the planet. As illustrated in Fig. 4, for this case, the impact flux normalized to its global average shows the strongest latitudinal variations. When the projectiles encounter the planet parallel to the equatorial plane, the flux is predicted to be considerably greater at the equator than at the poles, and tends towards a cosine function. This is simply a consequence of the geometric projection of the planet's surface area onto the direction of the unperturbed incoming projectiles. For the case in which $\Gamma = 0$, the impact flux

at latitude λ normalized to the global average is simply $\varphi_b(\lambda) = \frac{4}{\pi}\cos(\lambda)$. In the opposite extreme where the projectiles encounter the planet perpendicular to the equatorial plane, more impacts are expected at the poles than at the equator. For $\Gamma = 0$, it is easily shown that $\varphi_b(\lambda) = 2\sin(\lambda)$. It can be seen that in comparison with the previous case, the amplitude of the latitudinal variation is larger.

As the gravitational influence of a planet increases (or as the approach velocity decreases), Γ increases, and the bolide's trajectories become more and more deviated by the planet. As a consequence, the impact flux becomes more homogeneous. In the limit where Γ goes to infinity, the impact flux will approach a constant value independent of latitude, and independent of i_∞.

For similar geometric reasons, the mean impact angle measured with respect to the surface shows the strongest latitudinal variations for $\Gamma \ll 1$. For $i_\infty = 0°$, the mean impact angle is smaller near the poles than the equator, whereas it is the opposite for $i_\infty = 90°$. When Γ increases, these latitudinal variations decrease. In the limit where Γ goes to infinity, the mean impact angle will be everywhere exactly equal to 45°. Alternatively, if we assume an isotropic distribution of encounter inclinations ($P(i_\infty) \propto \cos(i_\infty)$), the average impact angle will also be 45° for all latitudes, irregardless of the value of Gamma. We note that, as shown in Appendix B, the globally averaged impact angle on a planet will always be equal to 45°, for any Γ or i_∞.

The common assumption in the crater chronology literature that the impact flux on a planet's surface is everywhere the same could arise from two situations: either the inclination distribution of impacting objects is isotropic, or the average factor Γ for the planet is large. Fig. 1 suggests that the first case is probably not true. Furthermore, using typical approach velocities of 25, 20 and 10 km/s for Venus, the Earth and Mars, the values of Γ lie between 0.09 and 0.16. Thus, as quantified in the following section, we should expect some form of latitudinal variations in impact conditions to exist on the terrestrial planets.

3. Results

In this section, we describe the latitudinal variations in impact conditions associated with the terrestrial planets that are expected from our model of planet-crossing objects. First, we show the collision probabilities for these bodies in terms of the relative encounter velocity and encounter inclination. Following this, we calculate the latitudinal variations in impact flux, impact velocity and impact angle for Mercury, Venus, the Earth, the Moon and Mars. Finally, using these results, we calculate the expected latitudinal variations in cratering rate and the expected size-frequency distribution of impact craters.

For these calculations, we use the current orbital elements of the planets as listed in Lodders and Fegley (1998). As the orbital elements of Mars are known to vary substantially (e.g., Touma and Wisdom, 1993), we use the results of Laskar et al. (2004a) and consider a simulation where the variations in eccentricity and obliquity are explicitly modeled over the past 3 billion years. Time-averaged values of these variables are 0.069 for the eccentricity and 37.6° for the obliquity, in comparison with the current values of 0.093 and 25.2°. Lacking a model for variations in inclination over this time-period, we assume that their distribution is Gaussian with a mean value and standard deviation of 4.0° and 1.5°, respectively. This accounts approximately for the potential range of values that the martian inclination can reach over long time periods (see Armstrong et al., 2004).

As noted earlier, the cratering rate on the Moon is expected to have a longitudinal dependency since it is in a state of synchronous rotation (e.g., Morota and Furumoto, 2003; Morota et al., 2005). We ignore this effect here, and treat this body in a approximate way. Following Stuart (2003), we calculate the impact probabilities for the Moon as if it were an isolated body having an Earth-like orbit. This assumption supposes that the Earth does not change substantially the averaged encounter conditions with the Moon. Concerning the encounter velocities, it is clear that the presence of the Earth would give slightly higher values, but this effect is small enough to be neglected. From energy conservation considerations, it can be shown that if the initial velocity at infinity was u_∞, the object's velocity at the orbit of the Moon ($a_☾$) would be $u' = \sqrt{u_\infty^2 + 2GM_♁/a_☾}$, where $M_♁$ is the mass of the Earth. For $u_\infty = 10$ and 20 km s^{-1} we have $u' = 10.1$ and 20.05 km s^{-1}, respectively. More detailed simulations for the Moon will be presented in a forthcoming paper.

3.1. Planetary collision probabilities

Fig. 5 shows the impact probability distribution for each planet in terms of the relative approach velocity u_∞ and encounter inclination i_∞. For clarity, these images have been normalized to the maximum value for each planet. The mean encounter velocities and inclinations are tabulated in Table 2 for the cases plotted in Fig. 5, as well as the corresponding mean impact velocities and mean values of Γ.

In general, the approach velocity distributions shows a large range of values, which is dependent not only on the distribution of eccentricities and semi-major axes of the planet crossing objects, but also on the orbital velocity of the planet. For Mars, in contrast, the encounter velocity distribution is considerably more narrow. This is simply related to the fact that the majority of objects that encounter this planet have relatively low eccentricities, and hence average orbital velocities that are comparable to this planet.

Fig. 6 shows the marginalized probability distributions of i_∞. It is seen that, with respect to the isotropic distribution, where no latitudinal variations are expected, Mars, and to a lesser extent Mercury, present inclination distributions that will potentially enhance the impact flux towards the poles, in contrast with the Earth and the Moon. Given these probability distributions, it is noted that the magnitude of the latitudinal impact rates will depend upon the mass and radius of the planet.

By summing all the collision probabilities calculated in constructing the distributions shown in Fig. 5, dividing by the planet's surface area, and then normalizing by the value obtained for the Moon, we obtain the relative impact flux that each planet is subjected to, R_b (see Table 2). If we assume that the bolide size distributions are uncorrelated with their orbital elements (Stuart and Binzel, 2004), R_b would be independent of bolide size (though see Marchi et al., 2005). We note that our calculated value of R_b for the Earth of 1.62 is close to the value of 1.68 determined from observations in Ivanov (2006). The calculated R_b value of 1.87 for Mercury is close to the value of about 1.8 cited by Ivanov (2006), based on the simulations of Marchi et al. (2005), that used the same NEO model. Shoemaker et al. (1991) estimated from observations of Venus and Earth-crossers that the collision rate per unit area on Venus is 0.95 times the rate on Earth, whereas we find a value of 1.10. The calculated R_b value is presently 3.23 for Mars, whereas it is 2.83 when accounting for its secular orbital variations over the past 3 Ga. This latter value is equivalent to the value quoted by Ivanov et al. (2002).

Bottke et al. (2002) estimated that there are about 960±120 NEOs with magnitudes lower than 18. According to (Morbidelli et al., 2002), who estimated the dark/bright ratio of NEOs, this value translates to 855±110 NEOs larger than 1 km. Using this result, the absolute impact flux on the Moon is $1.83^{\pm 0.23} \times 10^{-15}$ km^{-2} yr^{-1}.

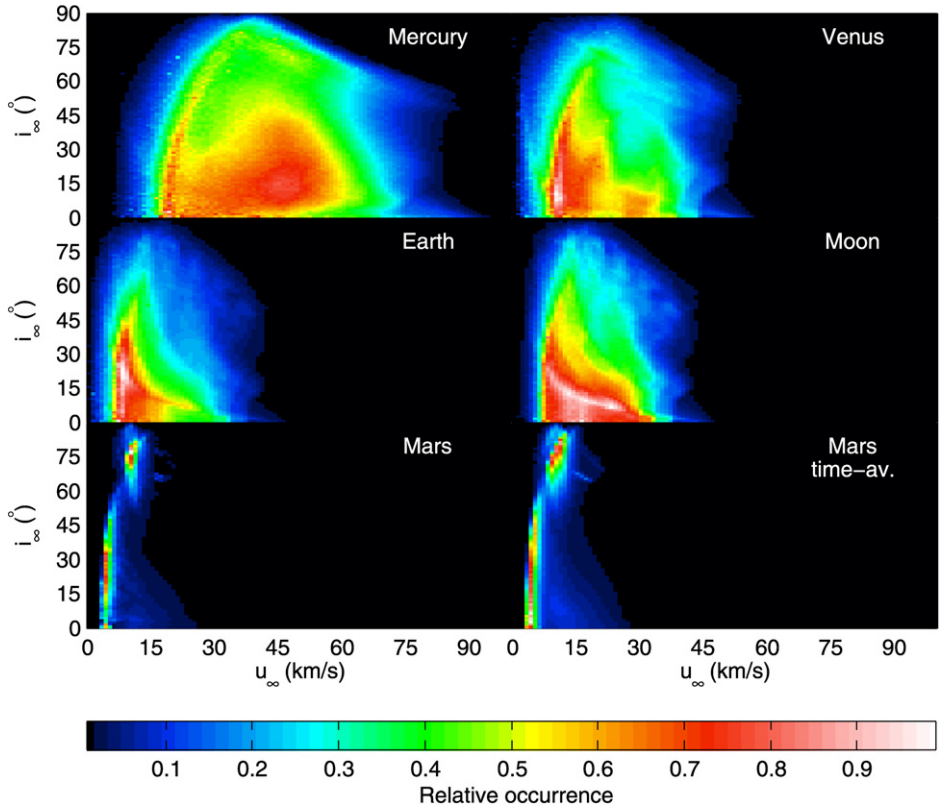

Fig. 5. Estimates of the collision probability for Mercury, Venus, the Earth, the Moon and Mars, as a function of the impactor's relative encounter velocity u_∞ and the inclination of this velocity vector with respect to the planet's orbital plane, i_∞. For Mars, collision probabilities are shown using both its current and time averaged orbital elements. Each plot is normalized to the maximum probability.

Table 2
Average cratering conditions on the terrestrial planets

Planet	Mercury	Venus	Earth	Moon	Mars	Mars (time-av.)
Mean approach velocity u_∞ (km s^{-1})	42.2	22.4	16.4	19.2	9.1	9.3
Mean Γ	0.01	0.48	0.94	0.02	0.29	0.29
Mean impact velocity u (km s^{-1})	42.5	25.2	20.4	19.4	10.6	10.8
Mean encounter inclination i_∞ (degrees)	34.1	32.7	30.2	30.0	41.5	41.0
R_b	1.87	1.79	1.62	1.00	3.23	2.83

3.2. Latitudinal dependence of impact conditions

The latitudinal dependencies of the relative impact flux normalized to the planet's global average, $\varphi_b(\lambda)$, are displayed in Fig. 7 for Mercury, Venus, the Earth, the Moon and Mars. The ratio of the polar to equatorial impact flux is seen to be 1.05, 1.00, 0.96, 0.90 and 1.26, respectively, using the current orbital parameters of these bodies. The primary cause for the differences in these latitudinal impact rates is the different encounter inclination distributions for these bodies. Whereas the encounter inclinations are biased towards low values for the Earth, Moon and Venus, a significant number of high inclination encounters occur for Mercury and Mars. By using the secular variations in the orbital history of Mars over the past 3 Ga, the pole/equator impact ratio is decreased to 1.14, which is almost entirely due to secular variations in this planet's obliquity. In the extreme case where we set the obliquity of Mars to 60°, the latitudinal effect is found to be negligible. We note that we can exactly reproduce the results of Halliday and Griffin (1982) (impact flux lower by 25% at the poles) when using their restricted set of orbits.

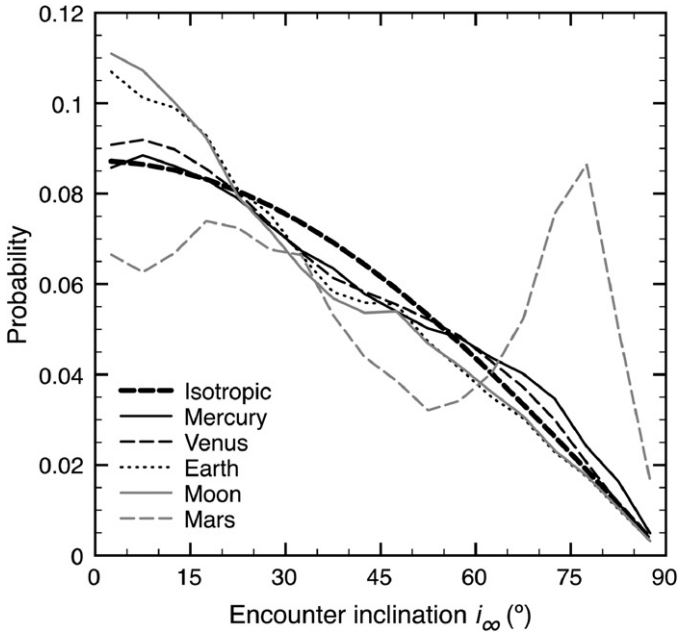

Fig. 6. Probability distribution of the encounter inclination i_∞ (angle of the relative velocity vector with respect to the orbit plane) for the terrestrial planets and Moon, compared to the isotropic case.

Fig. 8 shows the latitudinal dependencies of the mean impact angle measured with respect to the surface for the terrestrial planets and Moon. The mean impact angle is about 2.5° larger at the equator than at the poles for the Earth and the Moon. In contrast,

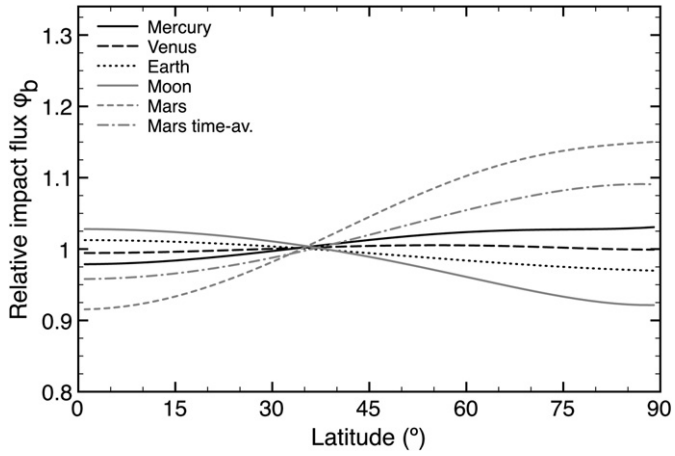

Fig. 7. Estimates of the impact flux as a function of geographic latitude on the terrestrial planets and Moon, normalized to the global average. Vertical scale is chosen for direct comparison with Fig. 9.

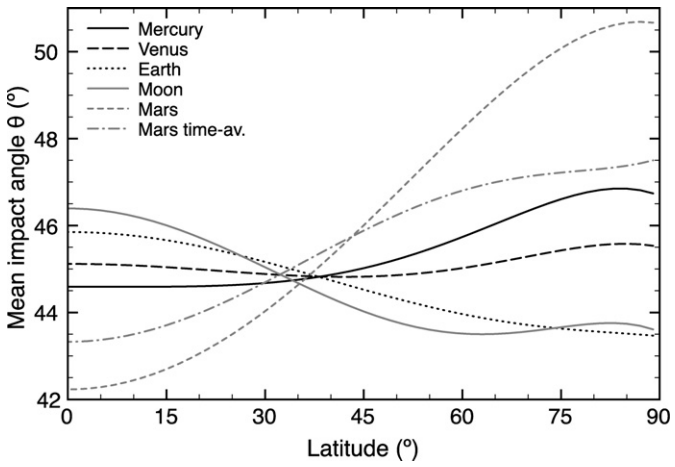

Fig. 8. Mean impact angle measured from the surface as a function of geographic latitude on the terrestrial planets and the Moon.

for Mercury, Venus and Mars, the mean impact angle is found to be larger at the poles by about 2°, 0.5° and 9°, respectively. By accounting for the secular orbital variations of Mars, the difference in mean impact angles is reduced by 5°. The mean impact velocity is relatively constant and varies only by about 0.2–0.5 $\mathrm{km\,s^{-1}}$ between the pole and the equator for all the objects of this study.

Even though the mean impact angle and impact velocity show well defined trends as a function of latitude, any single impact could have a value that differs significantly from the mean value. In particular, we note that for all cases investigated here, the standard deviation of the impact angle distributions is about 20° and the standard deviation of the impact velocity is between 35 and 45% of the mean value for all latitudes. The shape of the probability distribution of impact angle and impact velocity vary also with latitude. For example, impact events combining low impact angles and high velocities occur more frequently near the poles on the Moon. As a result, a greater proportion of craters would be expected to form with an impact angle less than 12° at high latitudes, and this would give rise to a larger number of elliptical craters (e.g., Bottke et al., 2000). For our Moon simulation, we found that there should be about 30% more highly oblique craters per unit area at the poles than at the equator. In contrast, the time-averaged Mars simulation gives the opposite result. As discussed in the following sections, a simple way to quantify the effects of the varying distributions of impact angle and impact velocity on the observed cratering record is by use of crater size-frequency distributions.

Finally, we comment further on the origin of the differences between the probability distributions in encounter inclination and velocity for the planets (Fig. 5), and hence their different latitudinal behavior. As described in Appendix A, the encounter inclination is given by Eqs. (A.6)–(A.8) as

$$\sin i_\infty = \frac{v}{u_\infty} \sin\alpha \sin i_{\mathrm{mut}} \tag{4}$$

where v is the object's velocity, u_∞ is the relative encounter velocity, α is the angle between the object's velocity vector and the Sun–planet vector, and i_{mut} is the mutual inclination. For Mars, whose distance from the Sun can reach 1.8 AU, Fig. 3 shows that a large number of encounters will occur with objects that are close to their perihelion, and for these objects, the probability of a collision is relatively large (see Appendix A). Such encounters naturally have large values of i_∞ for two reasons. First, α is near 90° and $\sin\alpha$ is hence close to 1. Second, the denominator of the prefactor u_∞ is smallest during encounters near perihelion since the angle between the two velocity vectors is minimized. This explanation also accounts, in part, for the slight surplus of high encounter inclinations for Mercury. Another effect for Mercury is that the objects that encounter this planet have higher than average orbital inclinations. Since the mutual inclination i_{mut} is approximately equal to the orbital inclination of the object (the inclination of Mercury is about 7°), the encounter inclination i_∞ will be on average larger than for Venus and the Earth.

3.3. Latitudinal cratering rates

Up until this point, we have discussed only the number of impacts that occur per unit area and unit time as a function of latitude (i.e., what we called the relative impact flux). However, when attempting to constrain the relative age of a surface, crater chronologists make use of the size-frequency distribution of impact craters. Instead of discussing impact fluxes (i.e., the number of objects that strike a planet per unit time), the relevant quantity to discuss is the cratering rate (i.e., the number of craters of size D that form per unit time).

Let us first consider cumulate distributions, and denote by $\dot{N}(>d,\lambda)$ the number of bolides larger than diameter d that impact the planet per unit time and unit area at a given latitude λ. If we assume that the size-frequency distribution of impacting objects does not change with time, we can write

$$\dot{N}(>d,\lambda) = \varphi_b(\lambda) T(t) \Phi_b(>d), \tag{5}$$

where φ_b is a function that takes into account latitudinal variations in the impact flux with respect to the mean value (see Fig. 7), T is a dimensionless function that takes into account temporal variations in the impact flux, and Φ_b is the present day average flux of objects striking the planet with diameters greater than d. Next, assume that a functional relation exists between crater diameter D and bolide diameter d of the form $d = d(D;u,\theta)$, which depends, among others, on the impact velocity and impact angle. If the probability of an impact occurring at a specific latitude is dependent on the impact velocity and impact angle, $P_\lambda(u,\theta)$, then the differential contribution to the cratering rate for a given u and θ can be expressed as

$$\mathrm{d}\dot{N}(>D,\lambda;u,\theta) = \varphi_b(\lambda) T(t) \Phi_b\big(>d(D;u,\theta)\big) P_\lambda(u,\theta). \tag{6}$$

The total cumulate number of craters larger than D that form per unit area and unit time (i.e., the cratering rate) is then simply

$$\dot{N}(>D,\lambda) = \int\int \mathrm{d}\dot{N}(>D,\lambda;u,\theta)\,\mathrm{d}u\,\mathrm{d}\theta, \tag{7}$$

and the cumulate number of craters on a planetary surface is the integral of the this function over time,

$$N(>D,t,\lambda)=\int_0^t \dot{N}(>D,\lambda)\,\mathrm{d}t, \tag{8}$$

where t is time before present. The corresponding differential size-frequency distribution of craters is simply given by the first derivative of its cumulative distribution:

$$n(D,t,\lambda)=\frac{\mathrm{d}N(>D,\lambda,t)}{\mathrm{d}D}. \tag{9}$$

In practice, this function is usually determined by counting the number of craters in a diameter bin of width $\sqrt{2}D$, and dividing by the bin width.

Equation (8) can be rearranged into a form that separates the time and latitudinal dependencies. By combining Eqs. (5)–(8) it is easily shown that

$$N(>D,t,\lambda)=\varphi_c(>D,\lambda)\big\langle\Phi_b(>d)\big\rangle\int_0^t T(t)\,\mathrm{d}t, \tag{10}$$

where the latitudinal dependence of the cratering rate is

$$\varphi_c(>D,\lambda)=\varphi_b(\lambda)\frac{\langle\Phi_b(>d)\rangle_\lambda}{\langle\Phi_b(>d)\rangle}, \tag{11}$$

and where $\langle\cdots\rangle$ denotes the expectation of the quantity over u and θ for d expressed as $d=d(D;u,\theta)$,

$$\big\langle\Phi_b(>d)\big\rangle=\int\int\Phi_b\big(>\mathrm{d}(D;u,\theta)\big)P(u,\theta)\,\mathrm{d}u\,\mathrm{d}\theta. \tag{12}$$

The subscript λ in Eq. (11) indicates that the expectation is to be performed using the velocity and impact angle distributions at a single latitudinal band, whereas the lack of a subscript indicates that the expectation should be performed over the entire planet. Similar expressions are easily derived for the differential size-frequency distribution.

The simulations in Section 3.2 give us the impact velocity and impact angle distribution P_λ. In order to calculate the size distribution of craters, we thus need to know the temporal variations in the bolide flux T, the size distribution of bolides $\Phi_b(>d)$, and the relationship between bolide and crater size. We will assume that the flux of impacting objects has been constant with time, and set T equal to 1. The size distribution of bolides is taken from Stuart and Binzel (2004) (J.S. Stuart, private communication). It is assumed that this distribution, estimated for NEOs, is also appropriate for Mercury, Venus, and Mars. As for the crater scaling, we will use equations that have been derived in the framework of π-scaling dimensional analysis (see Holsapple and Schmidt, 1987; Holsapple, 1993).

In the gravity regime, where the tensile strength of rock is negligible, the relationship between impact conditions and crater diameter for vertical impacts is of the form

$$\frac{D_\perp}{d}=K\left(\frac{u^2}{gd}\right)^{\nu_1}\left(\frac{\rho}{\rho_0}\right)^{\nu_2}, \tag{13}$$

where $D_\perp$ is the transient crater diameter for a vertical impact, d is the diameter of the impactor, ρ and ρ_0 are the density of the impactor and target, respectively, g is the surface gravity, and u is the impact velocity, all expressed in SI units. For non porous rocks, the adopted scaling constants are $K=1.17$, $\nu_1=0.22$ and $\nu_2=0.31$, whereas for dry sand $K'=1.03$, $\nu_1'=0.17$ and $\nu_2'=0.332$ (Schmidt and Housen, 1987; Holsapple and Housen, 2007). Small craters (less than about a kilometer) that form in the strength regime are simply proportional to the diameter of the bolide. Nevertheless, for simplicity, we will only consider simple and complex craters that form in the gravity regime.

The impact angle θ is known to affect the final crater size, though the functional dependence is not well quantified. Many workers consider that only the vertical component of the impact velocity contributes to the final crater size (e.g. Pierazzo et al., 1997). In contrast, laboratory experiments of Gault and Wedekind (1978) suggest that the volume of the crater formed is proportional to $\sin\theta$, and if the depth/diameter ratio of the crater does not change with impact angle, the crater diameter would be proportional to $(\sin\theta)^{1/3}$ (see Melosh, 1989). Many studies simply consider that all craters formed with vertical incidence (e.g. Shoemaker, 1983). It is clear from Fig. 8 that the mean impact angle varies as a function of latitude on the terrestrial planets. Thus, the cratering rate (which is dependent on crater size) will be sensitive to the manner in which oblique impacts are parameterized. We will assume that the transient crater diameter D_T depends upon incidence angle by the relationship

$$D_T=D_\perp(\sin\theta)^{\nu_3}, \tag{14}$$

and two cases will be considered. First, the transient diameter will be assumed to be independent of incidence angle by using $\nu_3=0$. Second, only the vertical component of the impact velocity will be assumed to influence the crater diameter by using $\nu_3=2\nu_1$. Each of the crater scalings described in the previous paragraph will give results between these two end-member cases.

Finally, craters larger than a critical diameter D_* are known to be modified by gravitational collapse of the crater walls, and this tends to increase the crater diameter. Such craters are referred to as complex craters, and D_* is the simple-complex transition diameter. As a first approximation, D_* can be considered to vary inversely proportional to the surface gravitational acceleration (Pike, 1980). For the Earth and Venus, D_* is about 3 km, whereas the corresponding diameters are 18 km for the Moon and 8 km for Mercury and Mars. The relationship between simple and complex craters is not well characterized, but the relationship of Croft (1985)

$$D=\begin{cases}D_T & \text{for } D_T<D_*,\\ D_*^{-\nu_4}D_T^{1+\nu_4} & \text{for } D_T\geqslant D_*,\end{cases} \tag{15}$$

with $\nu_4=0.18$, is commonly used.

In order to reconcile the size distribution of bolides with the average lunar crater size-frequency distribution of Neukum et al. (2001), we consider that craters with diameters less than a few kilometers form in the porous regime, as proposed by Ivanov (2006). The shape of the lunar crater size-frequency distribution is acceptably reproduced for crater diameters between 1 and 100 km by considering arbitrarily that porous scaling applies for $D<5$ km, whereas craters larger than 25 km formed in non-porous rocks. The transition between porous and non-porous scaling ($5<D<25$ km) is assumed to be linear. We further consider that the same transition applies to the other bodies of this study. Although the porosity of the lunar crust, and to a greater extent the crustal porosity of Mercury, Venus and Mars, are not well known, this assumption appears reasonable enough for our purposes.

The relative cratering rates normalized to the global average, $\varphi_c(>D,\lambda)$, calculated with the above equations and assumptions, are displayed in Fig. 9 for $D>1$ km. It is here considered that only the vertical component of the impact velocity contributes to the crater forming process ($\nu_3=2\nu_1$), which we believe is the most realistic case. As the impact angle is a function of latitude (see Fig. 8) that behaves in a similar manner as the impact flux (a larger flux at a given latitude is associated with a larger impact angle), the amplitude of the latitudinal variation is enhanced in terms of cratering rate (low impact angles create smaller craters). Our obtained pole to equator cratering ratios are summarized in Table 3, and

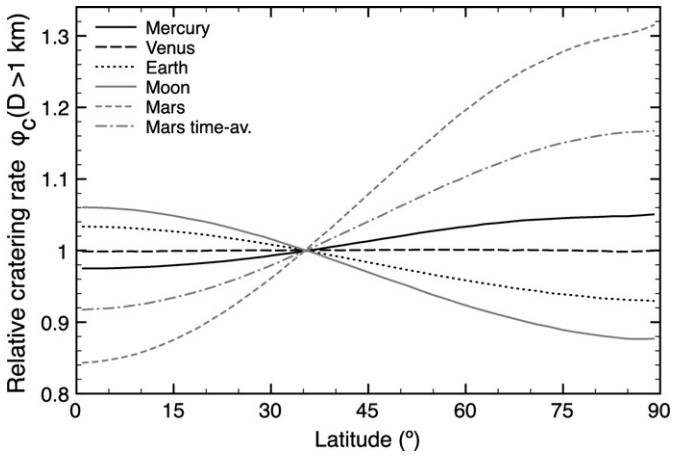

Fig. 9. Relative cratering rate variations with geographic latitude for crater larger than 1 km, on the terrestrial planets and the Moon. Crater scaling is done with the vertical component of the impact velocity.

Table 3
Pole/equator ratios of impact fluxes and cratering rates for $D > 1$ km

Ratio	Mercury	Venus	Earth	Moon	Mars	Mars (time-av.)
Impact flux	1.05	1.00	0.96	0.90	1.26	1.14
Cratering rate (1)	1.08	1.00	0.90	0.83	1.56	1.27
Cratering rate (2)	1.04	0.99	0.95	0.87	1.30	1.16

(1) Crater scaling with vertical component of impact velocity. (2) Crater scaling for vertical impacts.

compared to the case where the impacts are considered to be vertical ($\nu_3 = 0$). In this latter case, only the latitudinal variations in the impact velocity tend to increase the latitudinal asymmetry, but this effect is rather small. We note that Gallant et al. (2006), using four-body numerical simulations and crater scaling only for vertical impacts, report cratering rate ratios of 0.99 for the Earth and 0.91 for the Moon.

Although the latitudinal cratering rate, φ_c, is rigorously a function of D, we find that variations of less than 2–3% exist between the values reported in Table 3 for $D > 1$ km and values calculated for other diameters. For most practical purposes, $\varphi_c(\lambda)$ can be considered to be independent of diameter. This is illustrated in Fig. 10 where cumulative size-frequency distributions of craters are shown at the lunar pole and equator. Despite the different probability distributions in impact angle and velocity, the shape of the theoretical lunar size-frequency distributions is insensitive to latitude, and only a vertical offset between the curves is evident. The theoretical martian size-frequency distribution of craters, globally averaged over the planet's surface, is also shown to illustrate how the relative impact flux with respect to the Moon, R_b, and the different impact conditions on the two bodies (in particular, the impact velocity distribution), give rise to a differently shaped size-frequency distribution.

Also shown in Fig. 10 is Neukum's size-frequency distribution of lunar craters for a surface age of 3 billion years. In comparison, our calculated curves for a lunar impact flux $\Phi_b(d > 1\ \text{km}) = 1.83 \times 10^{-15}\ \text{km}^{-2}\,\text{yr}^{-1}$ are lower by a factor 4. The size-frequency distributions were calculated using Eqs. (10)–(15) with $\rho = 2050\ \text{kg m}^{-3}$ (corresponding to the mean density of lunar impactors estimated by Stuart and Binzel, 2004), $\rho_0 = 2700\ \text{kg m}^{-3}$ and $\nu_3 = 2\nu_1$. We note that in the crater scaling of Eq. (13), some authors consider an additional multiplicative factor of 1.56, accounting for both slumping and uplift during the crater formation process (Melosh, 1989). If we were to include this factor, our spatially averaged lunar SFD and the Neukum's production function would be almost perfectly superimposed over the considered diameter range, which would be consistent with a constant projectile flux during the last 3 billion years. Nevertheless, it should be noted that the assumption of a constant cratering rate over the past 3 Ga is debatable (see Hartmann et al., 2007), and considerable uncertainties exist with the current crater scaling laws and bolide size-frequency distributions.

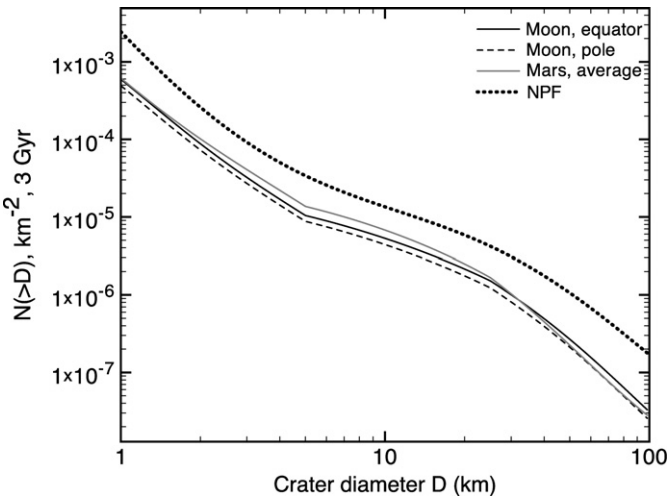

Fig. 10. Simulated cumulative size-frequency distributions of craters on the Moon (equator and pole) and Mars (globally averaged) for a surface age of 3 Gyr. The average lunar size-frequency distribution given by Neukum et al. (2001) is shown for comparison.

Finally, while $N(>D)$ is easily obtained for any arbitrary set of the above functions by numerical integration, if the cumulative number of objects greater than diameter d follows a power-law, simple analytic expressions exist that are useful for demonstration purposes. The size distribution of bolides is often assumed to be of the form

$$\Phi_b(>d) = \Phi_b(>1)d^{-m}, \tag{16}$$

where $\Phi_b(>1)$ is the average present-day flux of objects greater than 1 meter in size that strike the planet and m is the slope of the cumulative size-frequency distribution.

By inserting Eqs. (15)–(16) into Eq. (7), it is straightforward to show that the number of complex craters forming per unit time and unit area greater than diameter D is

$$\dot{N}(>D,\lambda) = \varphi_c(\lambda)\Phi_c(>1)D^{-s/(1+\nu_4)}, \tag{17}$$

where

$$\Phi_c(>1) = \Phi_b(>1)\left[\frac{K}{D_*^{\nu_4/(1+\nu_4)}g^{\nu_1}}\left(\frac{\rho}{\rho_0}\right)^{\nu_2}\right]^s\left\langle\left(u^{2\nu_1}\sin^{\nu_3}\theta\right)^s\right\rangle, \tag{18}$$

the latitudinal dependence of the cratering rate, which is here independent of D, is

$$\varphi_c(\lambda) = \varphi_b(\lambda)\frac{\langle(u^{2\nu_1}\sin^{\nu_3}\theta)^s\rangle_\lambda}{\langle(u^{2\nu_1}\sin^{\nu_3}\theta)^s\rangle}, \tag{19}$$

and

$$s = \frac{m}{1-\nu_1}. \tag{20}$$

The differential size-frequency distribution of the cratering rate is simply

$$\dot{n}(D,\lambda) = \frac{\mathrm{d}\dot{N}(>D,\lambda)}{\mathrm{d}D} = \frac{s}{1+\nu_4}\varphi_c(\lambda)\Phi_c(>1)D^{-\left(\frac{s}{1+\nu_4}+1\right)}. \tag{21}$$

It can be shown that Eqs. (17)–(21) are also valid for simple craters ($D < D_*$) by setting ν_4 equal to zero. In this case, the slope of the cumulative distribution is simply s.

Table 4
Relative average impact flux and cratering rates with respect to the Moon

Planet	Mercury	Venus	Earth	Moon	Mars	Mars (time-av.)
R_b	1.87	1.79	1.62	1	3.23	2.83
$R_c(>1\text{ km})$	2.6	1.0	0.7	1	1.2	1.1
$R_c(>20\text{ km})$	3.6	1.7	1.2	1	1.4	1.2

3.4. Interplanetary comparison

In order to date the age of a planetary surface using the crater counting method, it is necessary to extrapolate from the lunar cratering record that has been absolutely calibrated. In particular, one needs to take into account the different impact fluxes between the Moon and planet, and compensate for differences in impact conditions, such as the mean impact velocity and surface gravity. In this section, we briefly discuss how one can additionally take into account latitudinal variations in the impact flux and impact conditions.

The relative cratering rate between two planets is easily calculated by taking the ratio of their respective differential or cumulative size-frequency distributions. We use here the differential form and calculate the relative cratering rate as a function of latitude λ on a planet with respect to the average cratering rate of the Moon for a diameter D:

$$r_c(D,\lambda) = \frac{\mathrm{d}\dot{N}(>D,\lambda)/\mathrm{d}D}{\mathrm{d}\dot{N}_{\leftmoon}(>D)/\mathrm{d}D}. \tag{22}$$

While the cratering rate of the Moon is expected to vary with both latitude and longitude, we will assume that these effects have been taken into account when calculating the average lunar cratering rate. We next assume that the size-frequency distributions of the bolide fluxes for the two bodies are linearly related

$$R_b = \frac{\partial \Phi_b(>d)/\partial d}{\partial \Phi_b^{\leftmoon}(>d)/\partial d} = \frac{\Phi_b(>d)}{\Phi_b^{\leftmoon}(>d)}. \tag{23}$$

By using the definitions of Eqs. (8) and (9), Eq. (22) can be written as

$$r_c(D,\lambda) = \varphi_c(D,\lambda) R_c(D), \tag{24}$$

where the latitudinal variation in the cratering rate is

$$\varphi_c(D,\lambda) = \varphi_b(\lambda) \frac{\langle \partial\Phi(>d)/\partial d \partial d/\partial D\rangle_\lambda}{\langle \partial\Phi(>d)/\partial d \partial d/\partial D\rangle}, \tag{25}$$

the average relative cratering rate is

$$R_c(D) = R_b \frac{\langle \partial\Phi(>d)/\partial d \partial d/\partial D\rangle}{\langle \partial\Phi(>d)/\partial d \partial d/\partial D\rangle_{\leftmoon}}, \tag{26}$$

and it is noted that d implicitly depends upon D, u, and θ. $R_c(>D)$ and $r_c(>D,\lambda)$ are easily obtained in a similar manner, by the use of cumulative distributions.

Our R_c values are tabulated in Table 4 for craters larger than 1 and 20 km, respectively, along with the relative impact fluxes R_b. Note that atmospheric shielding was not included in these estimates. In particular, R_c estimates for Venus are tabulated only for comparative purposes and must not be treated as realistic since the dense atmosphere of Venus affects the formation of craters with sizes up to a few tens of kilometers.

The expression for the relative cratering rate is dramatically simplified when the size-frequency distribution of the bolides follows a power law. In this case, the differential distributions are given by Eq. (21), and when the craters of diameter D on the planet and Moon are both simple or complex, Eq. (22) is

$$R_c(D) = R_b \frac{\langle (u^{2\nu_1}\sin^{\nu_3}\theta)^s\rangle}{\langle (u^{2\nu_1}\sin^{\nu_3}\theta)^s\rangle_{\leftmoon}} \left[\left(\frac{D_*^{\leftmoon}}{D_*}\right)^{\frac{\nu_4}{1+\nu_4}} \left(\frac{\rho_0^{\leftmoon}}{\rho_0}\right)^{\nu_2} \left(\frac{g_{\leftmoon}}{g}\right)^{\nu_1} \right]^s. \tag{27}$$

4. Discussion

4.1. Isotropic comets

The Bottke et al. model does not include isotropic comets, as no such discoveries with periapses less than 1.3 AU were made by the Spacewatch survey. Nevertheless, some investigators have suggested that these could contribute from 10 to 30% of the observed terrestrial impact flux (see Weissman, 1990; Shoemaker, 1983; Zahnle et al., 1998). For our purposes, we note that the inclusion of a truly isotropic population of comets would act to minimize any latitudinal variations that might be present. It is simple to show that the relative impact flux at a latitude λ that includes the isotropic comets contribution would be

$$\varphi_{\mathrm{ic}}(\lambda) = \frac{\varphi_b(\lambda) + C_{\mathrm{ic}}}{1 + C_{\mathrm{ic}}}, \tag{28}$$

where C_{ic} is the fraction of the average impact flux resulting from isotropic comets. For example, for a polar/equatorial ratio of 0.90 (as we calculate for the Moon), the inclusion of an additional 20% of isotropic comets would reduce this factor to 0.92.

More recent estimates of the isotropic comet population, however, suggest that these are not as important as once believed. Strokes et al. (2003) estimated that the average impact energy of a long-period comet would be only 30% more than a NEA with a similar size. Using this result, as well as methods described in Marsden (1992) and Sekanina and Yeomans (1984), they showed that long-period comets represents only about 1% of the NEA cratering.

4.2. Observations

We next demonstrate that our calculated latitudinal variations in cratering rate are consistent with the observed cratering records for a few of the planetary objects investigated in this study. A detailed investigation involving the measurement of size-frequency distributions as a function of latitude on similar geologic units is beyond the scope of this article, and we instead analyze the global distribution of craters on the Moon and Venus using publicly available crater databases. We did not attempt to investigate the latitudinal variations of crater density for Mars because both the polar regions and northern hemisphere are geologically young when compared to large portions of the planet, and this would have biassed such a study. For the Earth, there are only a small number of craters, and the spatial distribution of these have been affected by both plate tectonics and true polar wander. Finally, we are not aware of a suitable database of craters for Mercury.

4.2.1. Venus

With the exception of a few ambiguous cases, all craters have been located on the planet Venus using Magellan SAR imagery (see Phillips et al., 1992). It has previously been shown that the spatial distribution of impact craters cannot be distinguished from a random distribution (Strom et al., 1994), which is in agreement with our results that predict a near zero latitudinal dependence. However, given the small number of craters, and the large counting statistics uncertainties, it would not be a simple matter to test any hypothesis concerning the latitudinal dependence of the cratering rate on this planet.

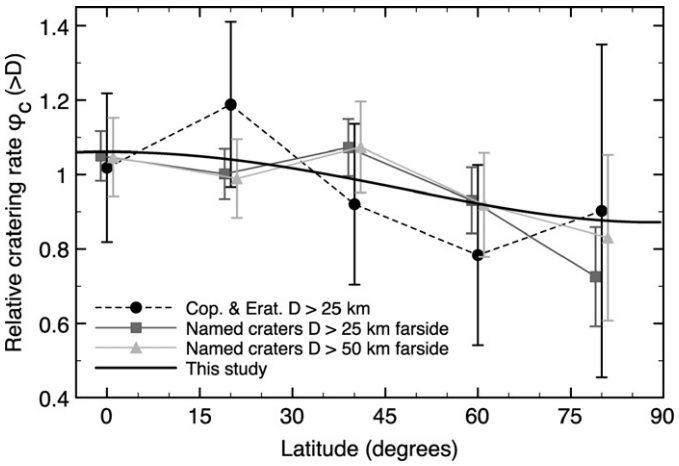

Fig. 11. Relative density of named craters larger than 25 km (dark gray squares) and 50 km (light gray triangles) on the farside of the Moon, and the relative density of Copernican and Eratosthenian craters larger than 25 km over the whole surface of the Moon (black circles). Our calculated relative cratering rate is shown for comparison.

4.2.2. Moon

We use the database[2] of "named" craters compiled by J. McDowell that is based on the database of Andersson and Whitaker (1982). As not all of the craters on the Moon have been named, we restrict ourselves to those that are greater than 25 or 50 km, anticipating that these subsets will be relatively complete. Since the spatial resolution of the farside highlands generally degrades towards the poles (see Plate 2 of Wilhelms et al., 1987), the difference between the >25 and >50 km datasets should be a relative indication of the completeness of these subsets of the database.

The geologic history of the nearside of the Moon is complicated by the presence of ancient highlands and young maria. We thus restrict this preliminary investigation to the farside highlands, which conceivably could have been affected by the same geologic processes over the past 4.5 Ga. In order to avoid complications with the Orientale and Australe basins, we further restrict this investigation to the longitudinal range 100–250 E. These criteria leave a total of 1349 and 539 craters that are greater than 25 and 50 km, respectively. In order to reduce the uncertainties with these estimates, we have combined craters in the northern and southern hemispheres, and have averaged the number of craters in 30 latitudinal bands. These results are plotted in Fig. 11. We additionally plot the number of Copernican and Eratosthenian craters larger than 25 km on the whole surface of the Moon (127 craters), using data provided by N. Petro, which is a compilation of data from Wilhelms et al. (1987), Grier et al. (2001), McEwen et al. (1993) and McEwen and Robinson (1997). For comparative purposes, we plot our predicted cratering rate using the same crater scaling laws as in Fig. 9. As is seen, all the observed densities show a tendency to be smaller near the poles than the equator, consistent with the theoretical results. Nevertheless, given the large uncertainties associated with the limited number of craters, and the shortcomings of the employed database, we can only say that the data suggest, but do not require, a latitudinal variation in the cratering rate. Furthermore, it must be noted that the size-frequency distribution of bolides that impacted the Moon prior to about 3.9 Ga could have been different than the current population of objects (see Strom et al., 2005).

[2] http://www.planet4589.org/astro/lunar.

4.3. Sensitivity to low inclination objects

As noted previously, the Bottke et al. model is discretized in 5° of inclination. Considering that the impact probability between an object and a planet is inversely proportional to the sine of their mutual inclination $i_{\rm mut}$ (see Appendix A), encounters with very low mutual inclinations will be highly probable. It is thus prudent to determine how sensitive our R_b values and impact flux distributions are to the exact form of the NEO model for the lowest inclinations.

We note that the relative impact fluxes of Mercury, Venus, and Mars should not be too sensitive to the form of the NEO model for the lowest inclinations. As the orbit planes of these planets are inclined to the ecliptic and precess, very little time will be spent when the mutual inclination with a planet-crossing object is zero. However, as already noted in Section 2.1, the inclination of the Earth's orbit is always close to zero, and any NEOs that exist with near-zero inclinations will thus have a high probability of impacting the Earth. As a result of this, the NEOs should be depleted at low inclinations, and to first order, one should expect the number to vary as $\sin i$.

We here compare our treatment of the lowest inclinations with other possible approximations. First, we assume that all objects in each (a, e, i) bin have inclinations equal to the cell's mid-point, an approximation that is in general used (e.g., Stuart and Binzel, 2004). Doing this, the absolute lunar impact flux is enhanced by about 3%. We note that the R_b values obtained from these two approaches are very similar, and differ by only 1% for Venus, the Earth and time-averaged Mars. In contrast, a slightly greater discrepancy of 3 and 4% exists for Mercury and the present-day Mars, respectively. The calculated latitudinal variations in the impact flux are found to be nearly identical using this approximation. Pole-to-equator ratios for the Earth, Moon and Mars are unchanged, whereas those for Mercury and Venus differ by only about 1 and 2%, respectively.

We next consider the case where the number of NEOs are uniformly distributed in each bin. While the latitudinal variations in the impact flux only change by about 1% for Mercury, Venus, and Mars, the results for the Earth and Moon are much different: with respect to the equator, the polar cratering rates are found to be about 10% less for the Earth and 50% for the Moon, in contrast to our previously reported values of 4 and 11%, respectively. The cause of this discrepancy is that this approximation artificially overemphasizes the number of near-zero inclination NEOs, which have a high probability of impacting the Earth and Moon. While the Earth/Moon impact ratio remains the same, their global impact fluxes are enhanced by a factor of about 1.8, and this causes the R_b values of the other planets to be decreased by this same factor.

As discussed in Section 2.2, we do not consider the approximation that the number of NEOs are uniformly distributed in each of the lowest inclination bins to be reasonable. Nevertheless it does demonstrate that there is a fundamental uncertainty in such modeling that does not appear to have been fully appreciated in previous studies. Current NEO models are deficient in both the number of observations at low inclinations, as well as the (a, e, i) resolution of debiased models. Future attempts to improve upon the relative impact fluxes between planets will require higher (a, e, i) resolution models than are currently available.

4.4. Temporal variations in the cratering rate

All of the terrestrial planets experience some secular variations in their orbital elements, and this will give rise to secular variations in their respective cratering rates. For Mars, long-term statistical analyses of the martian orbit have been performed by Laskar et al. (2004a). For the other planets, published analyses are

only available for smaller time periods. According to Laskar (1994), Mercury experiences very strong eccentricity and inclination variations, up to about 0.4 and 10°, respectively. The eccentricity and inclination variations of Venus and the Earth are moderate, but still amount to about 0.02 and a few degrees.

In addition to Mars, which was previously described in the text, we have also tested how secular variations affect the cratering rates of the Earth–Moon system, Venus and Mercury. The secular variations in inclination, eccentricity and obliquity over 250 Myr for the Earth and Moon were taken from Laskar et al. (2004b), whereas secular variations of Venus and Mercury were roughly reproduced over the past 10 Myr as plotted in Laskar (1988). Our results show that secular variations cause the impact flux and latitudinal effect to vary by less than 2%. Even though the secular variations of Mercury are large, the global impact flux is found to be nearly constant for this planet.

As a consequence of the above tests, the latitudinal variations predicted for the present day should be considered as good estimates for the planets' long-term behavior. Nevertheless, it should be noted that the NEO model of Bottke et al. (2002) and the observed Mars-crossers population, which are a fundamental input to our simulations, could be affected by secular variations in the planet's orbital parameters, as higher impact probabilities for certain (a, e, i) triads translates into a faster depletion of objects in this region of phase space. However, given the discretization size of the NEO model cells, moderate secular orbital variations of Venus and Earth would not be expected to affect significantly the orbital distribution of planet crossing objects. Nevertheless, as was pointed out by Ivanov (2001), a modulation of the orbital distribution of Mars crossing objects with the evolution of the martian orbit is possible. However, since the timescale for secular variations of the martian orbit (about 2 Ma) is shorter than the typical residence time for most Mars-crossers (about 30 Myr, Migliorini et al., 1998; Morbidelli, 1999), time variations of the Mars-crossing population would not be expected to be dramatic. Concerning the affects on the NEO population, it is noted that the contribution of the Mars-crossing source region in the Bottke et al. model accounts for secular variations of the martian orbit. It is possible, though, that variations of the martian eccentricity may affect more profoundly the whole resonance efficiency within the main belt.

Finally, we note that temporal variations in the absolute impact flux experienced by the planets are possible. Such short-term variations are expected to occur following collisions in the asteroid belt, especially when the collisions occur close to a primary resonance, and longer term variations in the isotropic comet flux are conceivable. In particular, Hartmann et al. (2007) suggest that the lunar cratering rate might have decreased by a factor of about 3 over the past 3 billion years. Culler et al. (2000) give a similar estimate, and suggest in addition that the cratering rate might have been substantially larger (by a factor 4) during the time of an asteroid breakup event about 500 Myr ago (see also Nesvorný et al., 2002). Time variations in the size-frequency distribution of planet crossing objects are also expected to occur following an asteroid breakup (Bottke et al., 2005; O'Brien et al., 2006). Beyond the past 3 Gyr, the consequences of a putative Late Heavy Bombardment on the orbital distribution of planet crossing objects and their size-frequency distributions are still unclear. The consequences of these phenomena to our model results are difficult to assess, but the calculated latitudinal variations may be considerably affected. To first-order we might expect that relative quantities between two planets, such as R_b and R_c, would be unaffected. Certainly, temporal variations in the impact flux, which are difficult to quantify, would hinder the determination of absolute ages of planetary surfaces by the crater chronology method.

5. Conclusions

In the absence of radiometrically dated samples, the size-frequency distribution of impact craters superposed on a geologic unit remains one of the few indicators that can be used to estimate both the absolute and relative chronology of geologic events on a given planet. One of the fundamental assumptions in most studies is that both the impact and cratering rates are spatially uniform across the planet's surface. Such a phenomenon would be expected if either the relative velocity distribution of planet-crossing objects were isotropic in space, or if the planet was sufficiently massive to deviate the trajectories of high encounter velocity objects.

By using a model of planet-crossing objects (which is based on a combination of Bottke et al.'s (2002) NEO model and the known asteroids) we have shown that the impact rate, impact angle distribution, and to a lesser extent the impact velocity distributions, are not spatially uniform across the surfaces of the terrestrial planets. Since the terrestrial planets are rotating, this effect gives rise to latitudinal variations in impact conditions. While the impact rates for Venus are nearly isotropic, the pole-to-equator impact rate for Mercury, Earth, the Moon, and Mars (the later of which accounts for secular orbital variations) are predicted to be 1.06, 0.96, 0.90, and 1.14, respectively. Using scaling relationships that relate the impact velocity, impact angle, and impactor size to final crater diameter, along with an estimate of the size-frequency distribution of impacting objects, latitudinal variations in the cratering rate are found to be somewhat larger. Pole-to-equator cratering rates for Mercury, Venus, Earth, the Moon, and Mars, accounting for secular orbital variations, are found to be 1.08, 1.00, 0.90, 0.83, and 1.27, respectively, for craters larger than 1 km. These ratios are nearly constant at all crater diameters between 1 and 100 km (variations are less than 3%), implying that, while the impact conditions vary as a function of latitude on a planet's surface, the size-frequency distributions of impact craters are nearly constant, with the exception of a simple vertical offset that depends on latitude.

If the globally averaged planetary cratering rates were constant in time, ages obtained from the crater chronology method would possess systematic latitudinal biases equal to the magnitude of the latitudinal cratering variations. As an example, a true age of 3 billion years on the Moon would appear to be about 2.6 and 3.2 billion years at the pole and equator, respectively. As the principal workers of the field caution that uncertainties in absolute ages derived by the crater chronology method are at best about a factor 2, these estimated latitudinal variations, though significant, lie within the absolute error bars of the methodology. Yet, they should be taken into account when calculating relative ages between two regions on the same body.

The results of our analysis depends upon several assumptions, though reasonable, that are difficult to assess in the absence of better data. Our calculated cratering rates depend upon the manner in which oblique impact conditions are incorporated into crater scaling laws, which are strictly valid only for vertical incidence conditions. The cratering rates also depends upon the assumed size-frequency distribution of planet-crossing objects, which may or may not be the same for each planet (see Marchi et al., 2005). Perhaps more importantly, though, we have assumed that both the size-frequency and orbital-element distributions of planet-crossing objects are in steady state, and are well described by the present-day distribution. We did not attempt to include planetocentric projectiles in our estimates. These are potentially major contributors to the cratering of the terrestrial bodies about 4 billion years ago (see Pinet, 1985). A higher resolution model of the orbital element distribution of planet-crossing objects, as well as estimates of the magnitude of its temporal variations, will ultimately be necessary in order to obtain more precise age estimates of planetary surfaces using the crater chronology method.

Acknowledgments

We thank W. Bottke for valuable discussions concerning the distribution of Near Earth Objects, as well as formal and informal reviews by B. Ivanov and J. Oberst.

Appendix A. Calculation of the planetary encounter probabilities and conditions

The methodology that we use to compute the probabilities of planetary encounters, as well as the encounter conditions, is based on the work of Greenberg (1982) and the modifications of Bottke et al. (1994). The necessary equations and approach are here summarized, and the interested reader is referred to these papers for further details.

Consider a planet (field body) and an asteroid or comet (test body) whose Keplerian orbits are described respectively by the triads (a_0, e_0, i_0) and (a, e, i), where a, e, and i refer to the semi-major axis, eccentricity, and inclination from the ecliptic of the two orbits. As described in Greenberg (1982), the collision probability represents the fraction of time for which the two bodies are close enough for a collision to occur, after averaging over all possible orbital orientations induced by the precession of the two orbits. This precession is assumed to be uniform, that is, the arguments of pericenter, ω and ω_0, and the difference between the longitudes of the ascending nodes, $\Delta\Omega$, vary uniformly with time. It is also assumed that the collision occurs near the mutual node of the two orbits, where the test body crosses the orbital plane of the field body.

The distance between the test body and the Sun is given by

$$r = \frac{a(1-e^2)}{1+eC}, \tag{A.1}$$

where C is the cosine of the true anomaly. The radius of the field orbit, r_0, is given by a similar expression, substituting a, e, i and C by a_0, e_0, i_0 and C_0. The distance between the two orbits is zero when $\mathbf{r} = \mathbf{r}_0$, that is

$$C = \frac{1}{e}\left[(1+e_0C_0)\frac{a(1-e^2)}{a_0(1-e_0^2)} - 1\right]. \tag{A.2}$$

Consider now the geometry of encounter described in Greenberg (1982) and shown for $\mathbf{r} = \mathbf{r}_0$ in Fig. A.1. The two bodies cross at O. The X axis is directed outward from the Sun, and the XY plane is the plane of the planet's orbit. The vectors $\mathbf{v}_0$ and $\mathbf{v}$ are the velocities of the field and test body, respectively. The angles α_0 and α are the angles the velocity vectors make with the X axis, which are given by

$$\cos\alpha = \frac{eS}{(1+2eC+e^2)^{1/2}} \tag{A.3}$$

and

$$\sin\alpha = \frac{1+eC}{(1+2eC+e^2)^{1/2}}, \tag{A.4}$$

where S is the sine of the true anomaly. The expressions are similar for α_0. The mutual inclination $i_{\rm mut}$, which is the angle between the two orbit planes, is

$$\cos i_{\rm mut} = \cos i\cos i_0 + \sin i\sin i_0\cos\Delta\Omega. \tag{A.5}$$

The sign of $i_{\rm mut}$ is chosen to be positive if the node of encounter is the ascending node, and negative otherwise (from symmetry considerations, the probability of collision at the ascending and descending node are equal). The velocity of the test body at the mutual node is given by

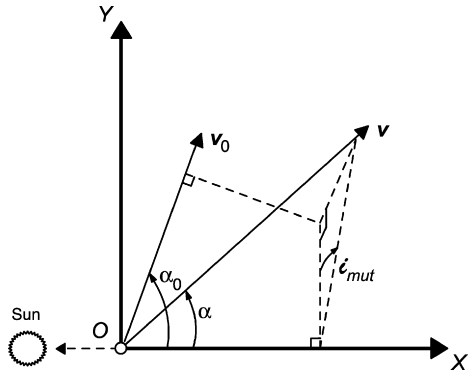

Fig. A.1. Geometry of encounter. The two bodies cross in O. The velocity $\mathbf{v}_0$ is in the XY plane, whereas $\mathbf{v}$ is not.

$$\begin{aligned} v^2 &= \frac{GM_\odot}{a(1-e^2)}\left(1+2eC+e^2\right),\\ v_x &= v\cos\alpha,\\ v_y &= v\sin\alpha\cos i_{\rm mut},\\ v_z &= v\sin\alpha\sin i_{\rm mut}, \end{aligned} \tag{A.6}$$

where $GM_\odot$ is the mass of the Sun times the gravitational constant. The velocity of the field body is given by

$$\begin{aligned} v_0^2 &= \frac{GM_\odot}{a_0(1-e_0^2)}\left(1+2e_0C_0+e_0^2\right),\\ v_{0,x} &= v_0\cos\alpha_0,\\ v_{0,y} &= v_0\sin\alpha_0,\\ v_{0,z} &= 0. \end{aligned} \tag{A.7}$$

The relative encounter velocity is then given by $\mathbf{u}_\infty = \mathbf{v} - \mathbf{v}_0$. The subscript ∞ accounts for the fact that the gravitational attraction of the planet is not included in the expression of the encounter velocity. The angle between the test body's relative velocity and the orbit plane of the planet, i_∞, is

$$\sin i_\infty = \frac{u_{\infty,z}}{u_\infty}. \tag{A.8}$$

The sign convention of i_∞ follows that of $i_{\rm mut}$, and the collision probability is the same whatever the sign of i_∞.

The expression for the collision probability is derived from the case $\mathbf{r} = \mathbf{r}_0$, and includes the width in the (C, C_0) space for which $\|\mathbf{r} - \mathbf{r}_0\| < \tau$, where τ is the radius of the collision cross-section, given by

$$\tau = R_0\sqrt{1+\frac{2GM_0}{R_0u_\infty^2}}, \tag{A.9}$$

with R_0 and M_0 being the radius and mass of the field body, and G the gravitational constant. Encounters with an impact parameter less than τ will lead to a collision. This approach implicitly assumes that the encounter velocity does not change significantly in the neighborhood of the mutual node. For a given ω_0 and $\Delta\Omega$, the collision probability per unit time, P_g, is finally given by (see Greenberg, 1982, for a complete and meaningful derivation)

$$P_g = \frac{\tau^2}{4\pi}\frac{A(1+eC)^2}{a(1-e^2)e|S|\sin i_{\rm mut}}\frac{B}{u_0T_0T}, \tag{A.10}$$

with

$$A = \left[\cot^2\alpha + \cot^2\alpha_0 + \sin^2 i_{\rm mut} - 2\cot\alpha_0\cot\alpha\cos i_{\rm mut}\right]^{1/2} \tag{A.11}$$

and

$$B = \frac{u_\infty}{[u_\infty^2 - (u_{\infty,x}\cos\alpha_0 + u_{\infty,y}\sin\alpha_0)^2]^{1/2}}, \tag{A.12}$$

where T and T_0 are the orbital periods of the test and field body. To get the total probability over all the possible orbital orientations, P_g must be evaluated at the four separate geometries corresponding to a single (C, C_0) couple (Bottke and Greenberg, 1993), then integrated over ω_0 and $\Delta\Omega$. As noted in Bottke et al. (1994), when the eccentricity and inclination of the field body are not zero, both the encounter velocity and inclination depend upon ω_0 and $\Delta\Omega$, and we consequently evaluate P_g, u_∞, and i_∞ for each of the four possible orbital orientations.

To construct the probability distribution of the relative encounter velocity and encounter inclination, $P(u_\infty, i_\infty)$, we first choose a test body with random values of a, e, and i. If its perihelion is less than the planet's aphelion, and if its aphelion is greater than the planet's perihelion, then a collision is possible and we proceed by choosing a random value of $\Delta\Omega$ between 0 and 2π, from which we compute $i_{\rm mut}$ from Eq. (A.5). Then, we choose randomly a value of C_0 within the range of permitted value imposed by the resulting value of C given by Eq. (A.2). From C, we obtain $S = \pm\sqrt{1-C^2}$, and choose the sign with equal probability. S_0 is calculated in a similar manner. The couples (C_0, S_0) and (C, S) give us one of the four possible collision geometries for a given ω_0, from which we calculate i_∞, u_∞ and P_g. As the value of P_g is singular when $i_{\rm mut} = 0$, we set $\sin i_{\rm mut} = \tau/r_0$ when $\sin i_{\rm mut} < \tau/r_0$, which is correct to third order in $i_{\rm mut}$ (Dones et al., 1999). Similarly, when the collision occurs near the periapse or apoapse of the test body, S tends towards zero and P_g goes to infinity. Following Greenberg (1982), this is cured by switching the definition of the field and test body. The collision probability P_g is finally weighted by the relative number of bodies in the corresponding bin of the Bottke et al. model, as given by Fig. 1. The values of P_g, u_∞, and i_∞ are tabulated, and this procedure is repeated until $P(u_\infty, i_\infty)$ converges.

Appendix B. Calculation of the impact conditions

In this appendix, we describe how we calculate the impact flux, impact angle, and impact velocity as a function of latitude on a planet for encounters with a given relative approach velocity and a given inclination of this velocity with respect to the planet's orbital plane. It is assumed that during the encounter phase, the trajectory of the impactor is not influenced by that of the Sun, and that the projectile as seen by the planet approaches from an infinite distance. If it is assumed that the spin rate of a planet is unrelated to the dynamics of the asteroidal and cometary orbits, the impact flux on a planet will only depend upon latitude.

According to symmetry considerations, we can consider that all bolides come from a single direction in space. For each (u_∞, i_∞), all projectiles that lie within the cross-section area τ will impact the planet (see Fig. B.1). We choose one such projectile uniformly on the plane perpendicular to the trajectory, by picking randomly the square of its impact parameter b between 0 and τ^2, and the rotation angle δ between 0 and 2π.

Consider the coordinate system (X, Y, Z) centered on the planet, the Y axis being in the direction of $\mathbf{u}_\infty$ and the X axis being chosen so that the XY plane contains the trajectory of the object. The initial position of the object is given by $X = b$ and $Y = -\infty$. The trajectory of the object is hyperbolic, and is described by

$$r = \frac{a(e^2-1)}{1+e\cos f}, \tag{B.1}$$

where r is the distance of the object from the center of the planet, a is the semi-major axis of the hyperbola, e its eccentricity and f the true anomaly. For an initial velocity u_∞ at an infinite radius, with an impact parameter b, the semi-major axis is given by

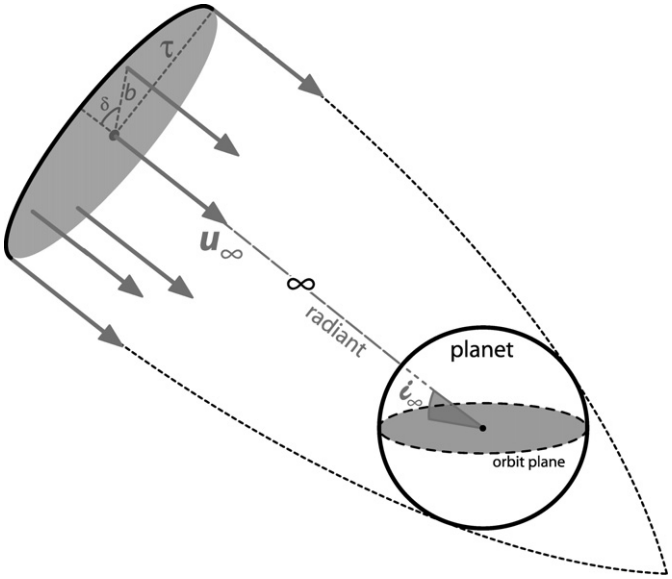

Fig. B.1. Schematic illustration of the bolides that will impact the planet for a given u_∞ and i_∞. The impact parameter b varies between 0 and τ, and the angle δ between 0 and 2π.

$$a = \frac{GM_0}{u_\infty^2}, \tag{B.2}$$

and the eccentricity is

$$e = \left(1 + b^2 u_\infty^4 / GM_0^2\right)^{1/2}. \tag{B.3}$$

The cosine of the true anomaly at launch point, f_∞, is

$$C_\infty = -1/e, \tag{B.4}$$

with the corresponding sine

$$S_\infty = -\left(1 - C_\infty^2\right)^{1/2}, \tag{B.5}$$

being negative, as $\mathbf{r}_\infty \cdot \mathbf{u}_\infty < 0$. The impact occurs at $r = R_0$, R_0 being the radius of the planet. From Eq. (B.1), the cosine of the true anomaly of impact, f_i, is

$$C_i = \frac{a(e^2-1)/R_0 - 1}{e}, \tag{B.6}$$

and the corresponding sine is given by

$$S_i = -\left(1 - C_i^2\right)^{1/2}, \tag{B.7}$$

where the sine of S_i discriminates between one of the two intersection points between the hyperbola and the planet. S_i is negative, as both S_∞ and S_i correspond to a time before the periapse, where by definition $f = 0$.

The coordinates of impact in the (X, Y, Z) frame are

$$\begin{aligned} X_i &= -R_0\cos(f_i - f_\infty) = -R_0(C_iC_\infty + S_iS_\infty),\\ Y_i &= R_0\sin(f_i - f_\infty) = R_0(S_iC_\infty + C_iS_\infty),\\ Z_i &= 0. \end{aligned} \tag{B.8}$$

We next obtain the geocentric coordinates of impact using the transformation

$$\mathbf{r}_{\rm geo} = M_{\rm obl}M_{\rm orb}\mathbf{r}_{XYZ}, \tag{B.9}$$

where $M_{\rm orb}$ is the rotation matrix from (X, Y, Z) to the coordinate system attached to the orbital plane of the planet, and $M_{\rm obl}$ the

rotation matrix from this latter to the geocentric coordinate system (attached to the planet's equatorial plane). We have

$$M_{\rm orb} = \begin{bmatrix} C_\delta & 0 & -S_\delta \\ S_i S_\delta & C_i & S_i C_\delta \\ C_i S_\delta & -S_i & C_i C_\delta \end{bmatrix}, \tag{B.10}$$

where C_δ and S_δ are the cosine and sine of δ, and C_i and S_i the cosine and sine of i_∞, and

$$M_{\rm obl} = \begin{bmatrix} C_\phi^2 + S_\phi^2 C_\epsilon & C_\phi S_\phi (1 - C_\epsilon) & -S_\phi S_\epsilon \\ C_\phi S_\phi (1 - C_\epsilon) & S_\phi^2 + C_\phi^2 C_\epsilon & C_\phi S_\epsilon \\ S_\phi S_\epsilon & -C_\phi S_\epsilon & C_\epsilon \end{bmatrix}, \tag{B.11}$$

where C_ϵ and S_ϵ are the cosine and sine of the obliquity of the planet (angle between the spin axis and the normal to the orbit), and C_ϕ and S_ϕ the cosine and sine of the angle ϕ. This latter angle is taken randomly between 0 and 2π, and simulates the fact that the spin axis can possess any orientation relative to the incoming direction of the projectile. It is finally straightforward to obtain the latitude of the impact site from the geocentric coordinates of impact.

The energy conservation gives the impact velocity as

$$u^2 = u_\infty^2 + v_{\rm esc}^2, \tag{B.12}$$

where $v_{\rm esc} = \sqrt{2GM_0/R_0}$ is the escape velocity at the surface of the planet.

The conservation of the specific angular momentum $\mathbf{h} = \mathbf{r} \times \mathbf{v}$ gives the impact angle θ. At the launch point, $h = bu_\infty$, whereas at the impact point, $h = \|\mathbf{r}_{\rm imp} \times \mathbf{u}\| = R_0 u \sin(\theta + \pi/2)$. Therefore,

$$\cos\theta = b/\tau. \tag{B.13}$$

Each object is launched for random values of b, δ and ϕ. This procedure is repeated until good statistics are obtained. The projectile flux at a latitude λ normalized to the global average is

$$\varphi_b(\lambda) = \frac{N(\lambda)}{N_{\rm tot}} \frac{4\pi}{(\sin\lambda^+ - \sin\lambda^-)}, \tag{B.14}$$

where $N(\lambda)$ and $N_{\rm tot}$ are the number of impacts at the latitude λ and the total number of impacts on the planet, respectively. The term $(\sin\lambda^+ - \sin\lambda^-)$ accounts for the area of the discrete latitudinal band between λ^+ and λ^-, whereas the term 4π accounts for the area of the sphere.

It can be seen from Eq. (B.13) that the impact angle θ can be expressed only as a function of the two dimensionless parameters $\Gamma = GM_0/R_0u_\infty^2$ and $B = b^2/R_0^2$. When calculating the impact angle distribution for a given disk of impactors, B varies uniformly between 0 and $1 + 2\Gamma$. It is therefore clear that the impact angle distribution depends only on Γ. Moreover, the mean impact angle on the planet is

$$\bar\theta = \frac{1}{1+2\Gamma} \int_0^{1+2\Gamma} \cos^{-1}\left(\frac{B}{1+2\Gamma}\right)^{1/2} {\rm d}B = \frac{\pi}{4}. \tag{B.15}$$

The globally averaged impact angle is thus always equal to 45° on any planet. Similarly, C_i and C_∞, and thus X_i and Y_i (Eq. (B.8)), can be easily expressed as functions of only Γ and B. Therefore, for a given obliquity ϵ_0, a disk of impactors with a given encounter inclination i_∞ will generate an impact flux at the surface of the planet that depends only on $\Gamma = GM_0/R_0u_\infty^2$.

References

Andersson, L.E., Whitaker, E.A., 1982. NASA catalogue of lunar nomenclature. NASA Reference Publication 1097.

Armstrong, J.C., Leovy, C.B., Quinn, T., 2004. A 1 Gyr climate model for Mars: New orbital statistics and the importance of seasonally resolved polar processes. Icarus 171, 255–271.

Bottke, W.F., Greenberg, R., 1993. Asteroidal collision probabilities. Geophys. Res. Lett. 20, 879–881.

Bottke, W.F., Nolan, M.C., Greenberg, R., Kolvoord, R.A., 1994. Velocity distributions among colliding asteroids. Icarus 107, 255–268.

Bottke, W.F., Love, S.G., Tytell, D., Glotch, T., 2000. Interpreting the elliptical crater populations on Mars, Venus, and the Moon. Icarus 145, 108–121.

Bottke, W.F., Morbidelli, A., Jedicke, R., Petit, J.-M., Levison, H.F., Michel, P., Metcalfe, T.S., 2002. Debiased orbital and absolute magnitude distribution of the near-Earth objects. Icarus 156, 399–433.

Bottke, W.F., Durda, D.D., Nesvorný, D., Jedicke, R., Morbidelli, A., Vokrouhlický, D., Levison, H.F., 2005. Linking the collisional history of the main asteroid belt to its dynamical excitation and depletion. Icarus 179, 63–94.

Croft, S.K., 1985. The scaling of complex craters. J. Geophys. Res. 90, 828–842.

Culler, T.S., Becker, T.A., Muller, R.A., Renne, P.R., 2000. Lunar impact history from ^{40}Ar/^{39}Ar dating of glass spherules. Science 287, 1785–1788.

Dones, L., Gladman, B., Melosh, H.J., Tonks, W.B., Levison, H.F., Duncan, M., 1999. Dynamical lifetimes and final fates of small bodies: Orbit integrations vs Öpik calculations. Icarus 142, 509–524.

Gallant, J., Gladman, B., Cuk, M., 2006. Current bombardment of the Earth–Moon system: Emphasis on cratering asymmetries. ArXiv Astrophysics e-print.

Gault, D.E., Wedekind, J.A., 1978. Experimental studies of oblique impacts. Lunar Planet. Sci. 9, 3843–3875.

Greenberg, R., 1982. Orbital interactions: A new geometrical formalism. Astron. J. 87, 184–195.

Grier, J.A., McEwen, A.S., Lucey, P.G., Milazzo, M., Strom, R.G., 2001. Optical maturity of ejecta from large rayed lunar craters. J. Geophys. Res. 106, 32847–32862.

Halliday, I., 1964. The variation in the frequency of meteorite impact with geographic latitude. Meteoritics 2, 271–278.

Halliday, I., Griffin, A.A., 1982. A study of the relative rates of meteorite falls on the Earth's surface. Meteoritics 17, 31–46.

Hartmann, W.K., Neukum, G., 2001. Cratering chronology and the evolution of Mars. Space Sci. Rev. 96, 165–194.

Hartmann, W.K., Quantin, C., Mangold, N., 2007. Possible long-term decline in impact rates. Icarus 186, 11–23.

Holsapple, K.A., 1993. The scaling of impact processes in planetary sciences. Annu. Rev. Earth Planet. Sci. 21, 333–373.

Holsapple, K.A., Housen, K.R., 2007. A crater and its ejecta: An interpretation of Deep Impact. Icarus 187, 345–356.

Holsapple, K.A., Schmidt, R.M., 1987. Point source solutions and coupling parameters in cratering mechanics. J. Geophys. Res. 92, 6350–6376.

Horedt, G.P., Neukum, G., 1984. Cratering rate over the surface of a synchronous satellite. Icarus 60, 710–717.

Ivanov, B.A., 2001. Mars/Moon cratering rate ratio estimates. Space Sci. Rev. 96, 87–104.

Ivanov, B.A., 2006. Cratering rate comparisons between terrestrial planets. LPI Contributions 1320, 26–27.

Ivanov, B.A., Neukum, G., Bottke, Jr., W.F., Hartmann, W.K., 2002. The comparison of size-frequency distributions of impact craters and asteroids and the planetary cratering rate. In: Asteroids III. Univ. of Arizona Press, Tucson, pp. 89–101.

Laskar, J., 1988. Secular evolution of the Solar System over 10 million years. Astron. Astrophys. 198, 341–362.

Laskar, J., 1994. Large-scale chaos in the Solar System. Astron. Astrophys. 287, L9–L12.

Laskar, J., Correia, A.C.M., Gastineau, M., Joutel, F., Levrard, B., Robutel, P., 2004a. Long term evolution and chaotic diffusion of the insolation quantities of Mars. Icarus 170, 343–364.

Laskar, J., Robutel, P., Joutel, F., Gastineau, M., Correia, A.C.M., Levrard, B., 2004b. A long-term numerical solution for the insolation quantities of the Earth. Astron. Astrophys. 428, 261–285.

Lodders, K., Fegley, B.J., 1998. The Planetary Scientist's Companion. Oxford Univ. Press, New York. 371 pp.

Marchi, S., Morbidelli, A., Cremonese, G., 2005. Flux of meteoroid impacts on Mercury. Astron. Astrophys. 431, 1123–1127.

Marsden, B.G., 1992. To hit or not to hit. In: Cavanan, G.H., Solem, J.C., Rather, J.D.G. (Eds.), Near-Earth Objects Interception Workshop. Los Alamos National Laboratory, Los Alamos, NM, pp. 67–71.

McEwen, A.S., Robinson, M.S., 1997. Mapping of the Moon by Clementine. Adv. Space Res. 19, 1523.

McEwen, A.S., Gaddis, L.R., Neukum, G., Hoffmann, H., Pieters, C.M., Head, J.W., 1993. Galileo observations of post-Imbrium lunar craters during the first Earth–Moon flyby. J. Geophys. Res. 98, 17207–17234.

Melosh, H.J., 1989. Impact Cratering: A Geologic Process. Oxford Univ. Press, New York. 245 pp.

Michel, P., Yoshikawa, M., 2005. Earth impact probability of the Asteroid (25143) Itokawa to be sampled by the spacecraft Hayabusa. Icarus 179, 291–296.

Migliorini, F., Michel, P., Morbidelli, A., Nesvorny, D., Zappala, V., 1998. Origin of multikilometer Earth- and Mars-crossing asteroids: A quantitative simulation. Science 281, 2022–2024.

Morbidelli, A., 1999. Origin and evolution of near-Earth asteroids. Celest. Mech. Dynam. Astron. 73, 39–50.

Morbidelli, A., Jedicke, R., Bottke, W.F., Michel, P., Tedesco, E.F., 2002. From magnitudes to diameters: The albedo distribution of near Earth objects and the Earth collision hazard. Icarus 158, 329–342.
Morota, T., Furumoto, M., 2003. Asymmetrical distribution of rayed craters on the Moon. Earth Planet. Sci. Lett. 206, 315–323.
Morota, T., Ukai, T., Furumoto, M., 2005. Influence of the asymmetrical cratering rate on the lunar cratering chronology. Icarus 173, 322–324.
Nesvorný, D., Morbidelli, A., Vokrouhlický, D., Bottke, W.F., Brož, M., 2002. The Flora family: A case of the dynamically dispersed collisional swarm? Icarus 157, 155–172.
Neukum, G., Ivanov, B.A., Hartmann, W.K., 2001. Cratering records in the inner Solar System in relation to the lunar reference system. Space Sci. Rev. 96, 55–86.
Öpik, E.J., 1951. Collision probability with the planets and the distribution of planetary matter. Proc. R. Irish Acad. Sect. A 54, 165–199.
O'Brien, D.P., Greenberg, R., Richardson, J.E., 2006. Craters on asteroids: Reconciling diverse impact records with a common impacting population. Icarus 183, 79–92.
Phillips, R.J., Raubertas, R.F., Arvidson, R.E., Sarkar, I.C., Herrick, R.R., Izenberg, N., Grimm, R.E., 1992. Impact craters and Venus resurfacing history. J. Geophys. Res. 97. 15923.
Pierazzo, E., Melosh, H.J., 2000. Understanding oblique impacts from experiments, observations, and modeling. Annu. Rev. Earth Planet. Sci. 28, 141–167.
Pierazzo, E., Vickery, A.M., Melosh, H.J., 1997. A reevaluation of impact melt production. Icarus 127, 408–423.
Pike, R.J., 1980. Formation of complex impact craters—Evidence from Mars and other planets. Icarus 43, 1–19.
Pinet, P., 1985. Lunar impact flux distribution and global asymmetry revisited. Astron. Astrophys. 151, 222–234.
Schmidt, R.M., Housen, K.R., 1987. Some recent advances in the scaling of impact and explosion cratering. Int. J. Impact Eng. 5, 543–560.
Sekanina, Z., Yeomans, D.K., 1984. Close encounters and collisions of comets with the Earth. Astron. J. 89, 154–161.
Shoemaker, E.M., 1983. Asteroid and comet bombardment of the Earth. Annu. Rev. Earth Planet. Sci. 11, 461–494.
Shoemaker, E.M., Wolfe, R.F., 1982. Cratering time scales for the Galilean satellites. In: D. Morrison (Ed.), Satellites of Jupiter. Univ. of Arizona Press, Tucson, pp. 277–339.
Shoemaker, E.M., Wolfe, R.F., Shoemaker, C.S., 1991. Asteroid flux and impact cratering rate on Venus. In: Lunar and Planetary Institute Conference Abstracts.
Stöffler, D., Ryder, G., 2001. Stratigraphy and isotope ages of lunar geologic units: chronological standard for the inner Solar System. Space Sci. Rev. 96, 9–54.
Strokes, G.H., Yeomans, D.K., Bottke, W.F., Chesley, S.R., Evans, J.B., Gold, R.E., Harris, A.W., Jewitt, D., Kelso, T.S., McMillan, R.S., Spahr, T.B., Worden, S.P., 2003. Report of the Near-Earth Objects Science Definition Team: A study to determine the feasibility of extending the search for near-Earth objects to smaller limiting diameters. NASA-OSS-Solar System Exploration Division.
Strom, R.G., Schaber, G.G., Dawsow, D.D., 1994. The global resurfacing of Venus. J. Geophys. Res. 99, 10899–10926.
Strom, R.G., Malhotra, R., Ito, T., Yoshida, F., Kring, D.A., 2005. The origin of planetary impactors in the inner Solar System. Science 309, 1847–1850.
Stuart, J.S., 2001. A near-Earth asteroid population estimate from the LINEAR survey. Science 294, 1691–1693.
Stuart, J.S., 2003. Observational constraints on the number, albedos, sizes, and impact hazards of the near-Earth asteroids. Ph.D. thesis, Massachusetts Institute of Technology, Cambridge, MA.
Stuart, J.S., Binzel, R.P., 2004. Bias-corrected population, size distribution, and impact hazard for the near-Earth objects. Icarus 170, 295–311.
Touma, J., Wisdom, J., 1993. The chaotic obliquity of Mars. Science 259, 1294–1297.
Weissman, P.R., 1990. The Oort cloud. Nature 344, 825–830.
Wetherill, G.W., 1967. Collisions in the asteroid belt. J. Geophys. Res. 72, 2429–2444.
Wilhelms, D.E., McCauley, J.F., Trask, N.J., 1987. The geologic history of the Moon. US Geological Survey Professional Paper 1348.
Zahnle, K., Dones, L., Levison, H.F., 1998. Cratering rates on the Galilean satellites. Icarus 136, 202–222.
Zahnle, K., Schenk, P., Sobieszczyk, S., Dones, L., Levison, H.F., 2001. Differential cratering of synchronously rotating satellites by ecliptic comets. Icarus 153, 111–129.